TAMPEREEN TEKNILLINEN YLIOPISTO
TAMPERE UNIVERSITY OF TECHNOLOGY

VILLE SALOMAA

EFFICIENCY STUDY OF AN ELECTRO-HYDRAULIC EXCAVATOR

Master's Thesis

Examiner: Professor Jouni Mattila
Approved by the Academic Board on
29 March 2017

ABSTRACT

VILLE SALOMAA: Efficiency Study of an Electro-Hydraulic Excavator
Tampere University of Technology
Master of Science Thesis, 59 pages, 16 Appendix pages
September 2017
Master's Degree Programme in Mechanical Engineering
Major: Fluid Power
Examiner: Professor Jouni Mattila

Keywords: Excavator, efficiency, hydraulics, displacement-control, valve-control, losses, throttle, mobile machinery, decentralization

Increasing regulation on emissions and a general trend towards more environmentally friendly solutions has motivated the researchers to look for ways to make mobile machinery more efficient. Excavators particularly are a remarkable source of pollution due to the vast amount and the low efficiency of these machines.

Excavators are ordinarily equipped with conventional, centralized hydraulic system, where main pump supplies volumetric flow for the whole system. This flow is directed from the pump to actuators through control valves, and the returning flow is directed into the tank. Conventional hydraulic system has numerous disadvantages. Many supportive functions are required, including pressure control and load-sensing functions. Even on idle mode, there are flow losses due to continuous circulation of fluid through valves. In addition, the distance between pumps and actuators may be long, which causes pressure loss and an additional weight of long hoses filled with fluid. One proposed improvement is the use of displacement-controlled hydraulics, in which the actuator control is realized by sophisticated pump control, instead of metering the flow in directional valves.

In this work, the efficiency of a modified JCB micro excavator is studied. Excavator is fitted with pressure and position sensors, and the simulation model is verified with laboratory measurements. The literature on the topic is reviewed to find the best practises concerning the studies on mobile machinery efficiency, including standardized duty cycles. The hydraulic system of the excavator is modelled in Matlab Simulink, and the simulation model is utilized to calculate the power consumption of the excavator during a digging and loading and a levelling cycle.

Further simulation study is produced by replacing the conventional hydraulic system with displacement-controlled units, namely direct-driven hydraulics, or DDH's. The same duty cycles are performed with both systems, and the results are presented. The study shows a power loss of as much as 60% in the directional valve group. A total power consumption of the DDH system is less than 10% of the consumption of conventional system, during two different free-space duty cycles. Subsequently, results of this study will motivate for further research and manufacturing a working prototype.

TIIVISTELMÄ

VILLE SALOMAA: Diplomityö
Tampereen teknillinen yliopisto
Diplomityö, 59 sivua, 16 liitesivua
Syyskuu 2017
Konetekniikan diplomi-insinöörin tutkinto-ohjelma
Pääaine: Fluid Power
Tarkastaja: professori Jouni Mattila

Avainsanat: hydrauliikka, kaivinkone, tehokkuus, kulutus, hajautettu järjestelmä

Päästömääräykset tiukentuvat ja teknisillä aloilla vallitsee yleinen suuntaus kohti yhä ympäristöystävällisempiä ratkaisuja. Tämä on ohjannut liikkuviin työkoneisiin liittyvää tutkimustyötä, sillä koneista halutaan nyt entistä energiatehokkaampia. Erityisesti kaivinkoneet aiheuttavat – koneiden suuren lukumäärän ja alhaisen hyötysuhteen takia – merkittävästi päästöjä.

Tyypillinen kaivinkone on edelleen varustettu perinteisellä keskitetyllä hydraulijärjestelmällä, jossa pääpumppu jakaa tilavuusvirtaa muulle järjestelmälle. Tilavuusvirta ohjataan pumpulta suuntaventtiilien kautta toimilaitteille, joilta saapuva paluuvirtaus johdetaan takaisin öljysäiliöön. Tällainen järjestelmä on monella tapaa epäedullinen. Se vaatii toimiakseen lukuisia aputoimintoja, kuten paineensäätöä ja kuormantuntotoimintoja. Jatkuva öljyn kierto venttiilien läpi aiheuttaa virtaushäviöitä jopa tyhjäkäynnillä. Pumpun ja toimilaitteiden välinen etäisyys on usein pitkä, joten letkuissa syntyy lisää virtaushäviöitä. Letkujen ja niiden sisältämän öljyn paino on koneen toiminnan kannalta ylimääräistä kuormaa. Ratkaisuksi näihin ongelmiin on esitetty tilavuusvirta- eli pumppuohjattua hydraulijärjestelmää, jossa järjestelmää ohjataan venttiilien sijaan älykkäällä moottorinohjauksella.

Tässä diplomityössä tutkitaan dieselistä sähkökäyttöiseksi muunnetun JCB Micro -kaivinkoneen energiatehokkuutta. Koneen hydraulijärjestelmä on mallinnettu Matlab Simulink -ympäristössä. Kaivinkoneeseen on asennettu paine- ja asema-anturit, joiden tuottaman mittausdatan avulla simulointimalli on verifioitu. Lisäksi esitellään aiheeseen liittyvää tieteellistä kirjallisuutta, josta on myös poimittu parhaita käytäntöjä liikkuvien työkoneiden tehokkuustarkastelua varten. Simulointimallin avulla selvitetään kaivunkoneen tehonkulutus kahden standardinmukaisen työsyklin aikana.

Vertailukohtana esitetään vastaavat tulokset vaihtoehtoiselle järjestelmälle, jossa perinteinen keskitetty hydraulijärjestelmä on korvattu pumppuohjatuilla, toimilaitteiden luo hajautetuilla yksiköillä. Samat työsyklit ajetaan molemmilla järjestelmillä. Tutkimus osoittaa, että venttiiliryhmässä syntyy jopa 60% koko järjestelmän tehohäviöistä. Pumppuohjatun järjestelmän energiankulutus on alle 10% perinteisen järjestelmän kulutuksesta, kun tarkastellaan kuormaamattomia työsyklejä. Työn tulokset ovat kiinnostavia ja ne kannustavat jatkotutkimukseen sekä prototyypin rakentamiseen.

PREFACE

Writing this thesis has been the ultimate goal of my studies, and the final task before graduating. During the last six months, I have learned more engineering skills than ever before. This challenging project threw me out of my comfort zone, time after time again. Getting this thesis done in time would not have been possible alone. It required the help from great colleagues, with whom I had the honor to work.

First, I want to thank professor Jouni Mattila, from Tampere University of Technology, for sharing his opinions and knowledge, and for helping me to set the scope for the work. I am thankful to the people of Aalto University, especially professor Matti Pietola, for providing me the opportunity to participate in EL-Zon project and work on my master's thesis with the most interesting topic. My supervisor, Dr. Tatiana Minav, steered me constantly into the right direction, and reminded me to write, write and write. And after the writing, she was always ready to review and comment the text, for which I am very grateful.

I also want to thank Olof, for spending countless hours in the lab, ordering vital components and especially for sharing his knowledge about the measurement systems. The practical work in the laboratory was full of challenges, which would have been difficult to overcome without the help of experts like Antti, Tuomas and Vadim. I am thankful for them, for making it possible for me to finish the project in time. The work on the simulation model formed a large part of the thesis. I am grateful for Shuzhong for all the discussions and help on the topic, and Jyrki for commenting my work and sharing his experience on modeling hydraulic systems.

My first roommates and colleagues, Tom and Aleksi, deserve a special thank for their invaluable and altruistic help in virtually any technical problem I ever had. I also want to thank the other co-workers: Tatjana, Abinab, Shayan, Shubu, Teemu, and Otto, for being such a hilarious lunch company; there is always blueberry pie for you.

Thank you, Pirita, for supporting me and for always finding ways to cheer me up. You make my life wonderful and good, and I am happy to share this achievement with you.

And thanks to my parents, Teija and Ilkka, and my brother Lauri, for being such a loving and encouraging family for me. I hope you are proud of me.

In Helsinki, Finland, on 10 September 2017

Ville Salomaa

CONTENTS

LIST OF SYMBOLS AND ABBREVIATIONS

AVEF	Auxiliary Valve Estimated Flow
ccm	Cubic centimeter (cm^3)
DC	Displacement controlled (hydraulic system)
DDH	Direct-driven hydraulics
EHA	Electro-hydrostatic actuator
EL-Zon	Electric-driven zonal hydraulics, a project funded by Tekes
IHA	Institute of Hydraulics and Automation, Tampere University of Technology
JCMAS	Japan construction machinization association
LS	Load-sensing (hydraulic system)
NI	National Instruments
NRMM	Non-road mobile machinery
ODE	Ordinary differential equation (solver)
PAV	Pressure adjustment valve
PVP	Pump side module (in Danfoss PVG32 valve)
PVB	Basic module (in Danfoss PVG32 valve)
PRV	Pressure relief valve

A	area	[m^2]
B_{eff}	effective bulk modulus	[Pa]
B_f	bulk modulus of the fluid	[Pa]
B_c	bulk modulus of a component	[Pa]
B_a	bulk modulus of insoluble air	[Pa]
C	flow coefficient	[-]
D	diameter	[m]
D_H	hydraulic diameter	[m]
F_c	Coulomb friction	[N]
F_s	static friction	[N]
F_μ	friction force	[N]
K_v	flow coefficient	[-]
l	length	[m]
P	power	[W]
p	pressure	[Pa] (1e5 Pa = 1 bar)
Δp	pressure differential	[Pa]
p_{nom}	nominal pressure differential	[Pa]
p_{tr}	transition pressure	[Pa]
q	volumetric flow	[m^3/s]
q_{nom}	nominal flow rate	[m^3/s]
Re	Reynolds number	[-]
Re_{tr}	transition Reynolds number	[-]
T	torque	[Nm]
u_{spool}	spool position	[-]
u_{ref}	reference signal	[-]
V	volume	[m^3]
ΔV	volume differential	[m^3]
V_a	volume of insoluble air	[m^3]
V_c	volume of a component	[m^3]

V_t	total volume of the system	[m^3]
v	velocity	[m/s]
v_s	Stribeck velocity	[m/s]
z	average deflection of bristles	[m]
λ	friction factor (pipe friction)	[-]
ε	Relative roughness of a pipe	[-]
ν	kinematic viscosity	[m^2/s]
ρ	fluid density	[kg/m^3]
σ_0	stiffness of bristles	[N/m]
σ_1	damping coefficient	[Ns/m]
σ_2	viscous friction coefficient	[Ns/m]
ω	rotational speed	[rad/s]
ω_n	natural frequency	[Hz]
ζ	friction factor (single loss)	[-]
ζ_d	damping ratio	[-]

.

1. INTRODUCTION

Non-road mobile machinery, or NRMM, covers a wide range of applications, including agriculture, earth-moving, and mining machinery. These machines are often utilized in challenging conditions, and their duty cycles consist of quick and high power peaks, which makes them a demanding target for research and development. Their requirement for high maximum power, along with full mobility, is why NRMM's are predominantly powered by a diesel engine. The rising fuel price, increasing regulation on emissions and a general trend towards more environmentally friendly solutions has motivated the researchers to look for ways to make the NRMM more efficient. Excavators particularly are a remarkable source of pollution. According to (Vukovic et al. 2017), the excavators would produce as much as 60% of all CO_2 emissions produced in construction machinery, due to the vast amount and the low efficiency of these machines.

Excavators are ordinarily equipped with conventional, centralized hydraulic system, which consists of one or two main pumps that supply volumetric flow for the whole system. This flow is directed from the pump to actuators through control valves, and the returning flow is directed into the tank. Conventional hydraulic system has numerous disadvantages. Many supportive functions are required, including pressure control and load-sensing functions. The power demand of the system changes, which prevents the engine from running at its optimal speed. Even on idle mode, there are flow losses due to continuous circulation of fluid through valves. In addition, the distance between pumps and actuators may be long, which causes pressure loss and an additional weight of long hoses filled with fluid.

In a load-sensing (LS) system, a load-sensing circuit monitors the load pressures on all actuators, and adjusts the system pressure to match the highest load. If several actuators operate at the same time, which often is the case, the excess pressure is decreased by throttling. According to (Zimmerman et al. 2007), these throttle losses may be responsible for as much as 35% of total energy losses during a typical digging cycle. Knowing the energy distribution of the machine is vital in order to steer the research towards the most relevant targets.

The first object of this study is to resolve the actual energy consumption and power distribution of the front hoe of the micro excavator (Figure 1), including boom, arm and bucket actuators. This is done by creating a simulation model in Matlab Simulink environment. Excavator is fitted with pressure and position sensors, and the simulation model is verified with laboratory measurements. The literature on the topic is reviewed to find the best practices concerning the studies on mobile machinery efficiency,

including standardized duty cycles. The simulation model is utilized to calculate the power consumption of the excavator during a digging and loading and a levelling cycle.

Figure 1: JCB Micro excavator

One solution for improving the efficiency of the excavator hydraulic system, is the use of displacement-controlled (DC) hydraulics, in which the actuators are controlled directly with the pump, instead of the directional valves. The direct-driven hydraulics (DDH) consists of two fixed displacement pump/motor units, which are connected to an electric motor via a common shaft. The ratio of pump displacements corresponds to the ratio of cylinder chamber displacements. However, since the pumps and cylinders are manufactured in standard sizes, there is usually some inequality between ratios, which is compensated with a hydraulic accumulator.

One task of the EL-Zon project is to replace micro-excavator front hoe hydraulics with three standalone DDH actuators. Findings can be projected into larger excavators and other multi-joint structures of the mobile machinery. Previous studies suggest that typical cycle control and potential energy recovery of a micro-excavator by DDH are feasible. Moreover, the research indicated that the overall efficiency of such setup could be as high as 76.4%. Comparable research data, concerning the conventional model, has not been available until now.

Further research on the simulation model is done by replacing the conventional hydraulic system with three DDH's. The same duty cycles are performed with both systems, and the results are presented. Predicted finding is that the efficiency of micro-excavator could be improved by replacing original hydraulics with DDH actuators. The scale of the

improvement is to be found out. From the overall view, an authentic simulation model is a vital part of DDH development process. Subsequently, results of this study are expected to motivate manufacturing a working prototype.

This structure of this thesis is as follows. In chapter 2, the previous research on efficiency of hydraulic mobile machinery is presented. Results of other studies offer valuable best practices and a basis to evaluate the results. The excavator and its modifications are described in chapter 3. In chapter 4, the simulation model is introduced in a detailed manner to ensure the reproducibility of all results. In chapter 5, the simulation model is utilized to study the power consumption of the excavator during two standardized working cycles. Both hydraulic systems, conventional and DDH, are investigated and the results are discussed. The final conclusions, together with suggestions concerning the upcoming research, are presented in chapter 6. Appendices include the description of the data acquisition and control system, measured dimensions of the front hoe, and the Matlab m-file including the model parameters.

The results of this thesis are being evaluated for publication: Salomaa, V., Minav, T., Mattila, J., Pietola, M. Efficiency Study of an Electro-hydraulic Excavator. 11th International Fluid Power Conference (IFK), Aachen.

2. LITERATURE REVIEW

Working machines in general and their efficiency in particular, form a widely researched field of science. Numerous studies have been published about improving the efficiency of mobile machinery. There are distinguishable research trends, such as hybridization of construction machinery, which was studied in detail in (Lin et al. 2010).

In this thesis, the focus is on the improvement of excavator efficiency by reducing the losses of the hydraulic system. In the literature review, some of the most relevant studies are introduced, and the best practices are adopted. In addition, results of preceding research form a basis for this study.

2.1 Efficiency of an excavator

Hydraulics are widely used in mobile machinery due to the good power-to-weight-ratio, or power density. It is also relatively flexible way to transfer power, because power can be moved through flexible hoses. Furthermore, hydraulic systems are capable of producing very high actuator forces and torques with the basic components, and the hydraulic system is very tolerant against overloading. However, the efficiency of a hydraulic system is only moderate. (Kauranne et al. 2008).

The excavator can be thought as an energy transformer. The input energy, whether it is stored in a battery or fuel, is first transformed into a mechanical energy. The mechanical power of a rotational system is determined as:

$$P = T \cdot \omega \qquad (1)$$

Notation	Explanation	Unit
P	power	W
T	torque	Nm
ω	rotational speed	rad/s

This mechanical energy, namely rotation of the electric motor or a diesel engine, is utilized to rotate the hydraulic pump. The hydraulic power is distributed to the actuators, which eventually output the mechanical work. Hydraulic power P[W] is given by:

$$P = q \cdot p \qquad (2)$$

Notation	Explanation	Unit
q	volumetric flow	m^3/s
p	pressure	Pa

Yet another form of mechanical power, the power of one-dimensional movement, occurs in this study. It is calculated by:

$$\boldsymbol{P = F \cdot v} \qquad \textit{(3)}$$

Notation	Explanation	Unit
F	force	N
v	velocity	m/s

The efficiency η can be calculated as a ratio between the power output and power input:

$$\boldsymbol{\eta = \frac{P_{out}}{P_{in}}} \qquad \textit{(4)}$$

Another interesting value in efficiency study, is the power loss over a single component. For example, a flow entering a valve has a hydraulic power P_{in}. The pressure drops due to throttling, so the output power, P_{out} is less than P_{in}. Now the power loss, or power spent in *heating* of the oil and the valve body, is

$$\boldsymbol{P_{loss} = P_{in} - P_{out}} \qquad \textit{(5)}$$

Depending on the component and the study objects, the definition of output power may vary. For example, a directional valve clearly outputs a volumetric flow for the use of other components, whereas the flow through a pressure relief valve is normally directed into the tank, and considered losses. In the latter case, the $P_{loss} = P_{in}$.

Since the power distribution and magnitude varies along the working cycle, it is expedient to calculate the total energy consumption during the cycle, and then compare the single values. Energy (E) is the integral of power over time, and its unit is Joule (J). For energy applies:

$$E_{in} = \int P_{in}\, dt, \qquad E_{out} = \int P_{out}\, dt, \qquad \eta = \frac{E_{out}}{E_{in}}, \qquad E_{loss} = \int P_{loss}\, dt \tag{6}$$

Energy studies on excavators in general are not straightforward, since the machines are fitted with a variety of auxiliary equipment, such as steering or cooling, which consume energy without contributing in productive work. Furthermore, the excavators are utilized in varying working cycles with different power consumption profiles. (Vukovic et al. 2017).

The excavator front hoe consists of multiple joints and actuators to provide freedom for different tasks. Besides different working positions and movements the excavator is facing, it also needs to work with different loads. Even the simplest digging cycle includes pressing (as the bucket penetrates into the soil) and pulling (as the bucketful of soil is being lifted up). In Figure 2, two possible directions of movement, extending and retraction, are combined with two different load directions, assistive and resistive load. Similar two-by-two matrix representation is presented in (Vukovic et al. 2017).

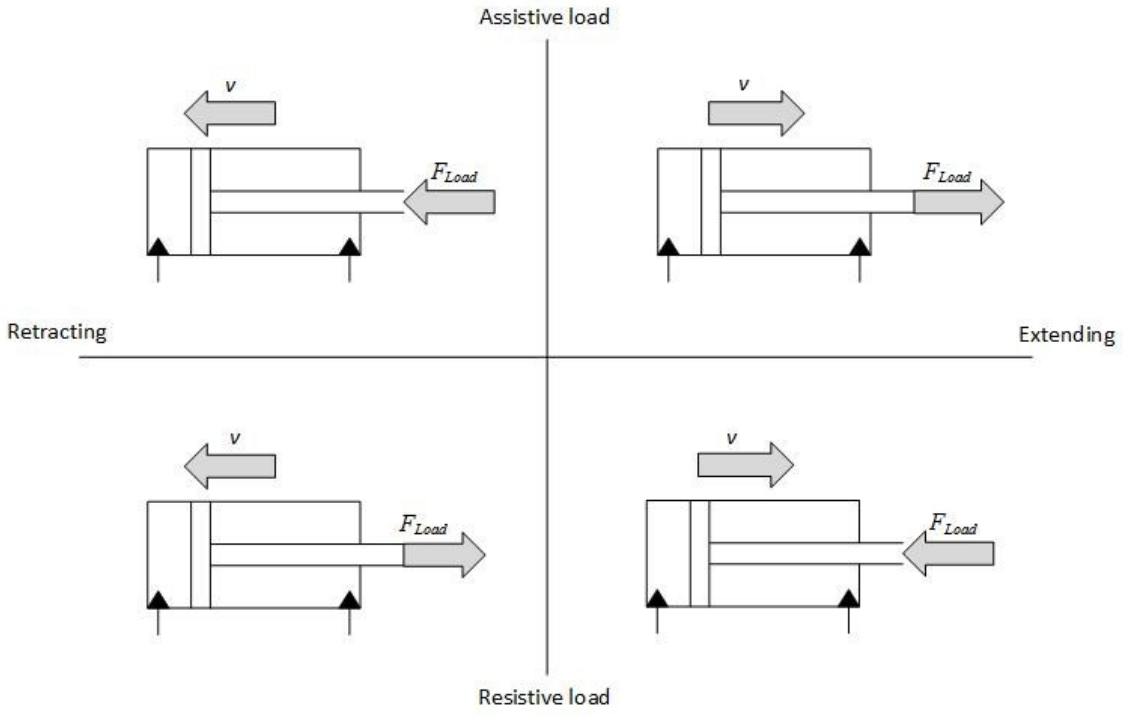

Figure 2: Four load situations (Vukovic et al. 2017)

As the figure illustrates, the loading conditions of the excavator actuators are variable and must be taken into account when determining the output work done by the actuator. This is further discussed in chapter 5: Efficiency analysis.

The term “individualization” was introduced in (Weber et al. 2016), to express the trend from centralized to decentralized (pump-controlled) hydraulic systems. In the least individualized systems, one pump-motor unit is commonly used by several actuators. This kind of system is usable in applications, where only one actuator works at a time, due to strict working sequence, for example. According to Weber et al., the next step in the individualization is to assign an own pump for each actuator, while still using a common motor. This kind of systems are found particularly in mobile machinery, as they commonly perform separate functions simultaneously. Even more individualized systems involve separate motor-pump units assigned to each actuator. Trend is towards structural integration of these individual cells, including motor, pump and the actuator. Compact electro-hydrostatic actuators (EHA), present a state of art technology in this field. EHA’s were originally taken into use in aircraft industry in the 1990’s and industrial applications in late 2000’s (Weber et al. 2016).

2.2 Displacement control in NRMM

At the same time, other researchers have focused on improving the efficiency of the hydraulic circuit. As mentioned, the directional valves cause a major part of all power losses in the system. A significant approach towards this problem is displacement controlled (DC) actuator, which is controlled directly by a variable displacement pump instead of directional valves. DC system is already a common solution in hydrostatic transmissions, but the unequal volumes of the differential cylinder have as of yet prevented it from spreading into other systems. However, variety of different approaches have been introduced to overcome this problem.

Electro-hydrostatic actuator (EHA) can be perceived as a subtype of DC systems. It involves a fixed displacement pump, driven by a variable speed electric motor. EHA is not hydraulically connected to the central system, instead, only electric wiring is required to connect it. Thus, the EHA has enabled progress towards a decentralization of the hydraulic system.

(Zimmerman et al. 2007) have studied the power consumption of a Bobcat 435 compact excavator, to identify the main causes of power loss, and discuss the benefits of a valve-less control. They created a Simulink model to simulate the dynamic behavior of the machine, and a mathematic model to calculate power losses by combining the flow rates and pressure drops of each component. Using a typical digging cycle, they found that only 31.4% of the total input energy (energy delivered by the engine) was captured into actuator work. As much as 35.2% was lost in the valve block, and 29.0% was used in the pump. The study highlighted a problem characteristic for a LS system, namely that in case of multiple simultaneous actuator movements, the system pressure is set according to the highest load. The flow for functions with lower pressure demand is heavily throttled, which leads to high energy losses.

The project goal of Zimmerman et al. was to use displacement controlled actuators, in order to reduce the total fuel consumption of the excavator. The DC actuators would not only lower the throttle losses, but also allow energy recovery, whenever the assistive load is applied. The authors estimated that 26.1% of the work and 8% of the total energy consumption is recoverable.

(Williamson et al.) have continued the work to compare the energy consumption of a conventional excavator and a displacement controlled excavator. The same mini-sized excavator, Bobcat 435, was investigated also in the latter project. The energy consumption and distribution was studied by using a simulation model, in which both the LS and DC systems were modeled.

Williamson's DC system was based on a variable volume pump, which directly operates a single-rod cylinder. The flow differential over the pump is compensated with pilot-operated check valves and an accumulator. Excess oil is directed to the tank, and returned with a supplementary pump. The application into the excavator incorporates on/off valves to connect multiple alternative actuators in a single circuit. For example, the same circuit may be used to control the boom cylinder and the right travel motor, since the functions are not used simultaneously.

Another difference between the study of (Williamson et al.) and this thesis is the application of external load. Williamson et al. utilized the measured pressure and position data, with friction and acceleration values acquired from the simulation model, to calculate an estimated load force, which was applied to the actuators during the simulation.

According to Williamson et al., a 39% reduction in power consumption is achievable with a DC system, compared to a conventional LS system. Valve metering losses, which are the greatest single source of power loss, were reduced by 99.3%. On the downside, the pump losses were more than doubled. One of the main arguments supporting the investigation for DC systems, energy recuperation, was found negligible.

2.2.1 Direct-driven hydraulics

A major design problem, related to pump-control of a single-rod cylinder, is how to balance the different volume flows of the two cylinder chambers. The direct-driven hydraulics (DDH) consists of two fixed displacement pump/motor units, which are connected to a common shaft with an electric motor. A simplified hydraulic schematic is presented in Figure 3. The ratio of pump displacements V_{rA} and V_{rB} corresponds to the ratio of cylinder chamber displacements, and, thus, piston areas A_{pA} and B_{pB}:

$$\frac{V_{rA}}{V_{rB}} \approx \frac{A_{pA}}{A_{pB}} \quad (7)$$

However, since the pumps and cylinders are manufactured in standard sizes, there is usually some inequality between ratios. To prevent unwanted pressure difference, caused by this inequality, there is an additional hydraulic accumulator placed between the cylinder and pump. According to study (Järf et al. 2016), this accumulator may improve the efficiency of this type of system by 30%. Another accumulator acts as an oil reservoir, enabling a tank-less configuration. The DDH forms a standalone unit, which may be installed close to the hydraulic cylinder, requiring only electric cables to connect it with the power source.

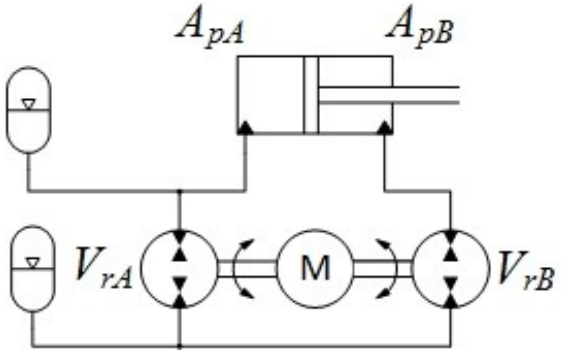

Figure 3: Schematics of a tank-less DDH unit

One task of the EL-Zon project is to replace micro-excavator front hoe hydraulics with three DDH actuators. Findings can then be projected into larger excavators and other multi-joint structures of the NRMM. In this thesis, a simulation model is created, in which the front hoe is actuated with three standalone DDH units. This system will be compared against the conventional one to observe the characteristics, such as efficiency and performance. Simulation models utilized to study the systems are produced using Matlab Simulink. In order to accomplish sufficiently accurate simulation, the model will be verified with in-situ measurements.

The DDH system of a micro-excavator has been modeled during previous studies in the EL-Zon project. The model consists of a multibody dynamic model, hydraulic model, and electric drive model. The simulation research suggested that typical cycle control and potential energy recovery of a micro-excavator by DDH are feasible. Moreover, the research indicated that the overall efficiency of such setup could be as high as 76.4%, which motivates further research.

2.3 Excavator duty cycles

In order to evaluate the performance or efficiency of an excavator, it is necessary to determine the actual use of such a machine. Digging movement is common to all duty cycles found in the literature. However, as explained in section 2.1, the varying loading conditions make standardizing a difficult task, as the excavators are used in very different conditions. Possibly the most commonly utilized duty cycle, presented by the Japan construction machinization association (JCMAS), solves the problem by determining unloaded, or free-space, duty cycles (JCMAS 2007).

2.3.1 JCMAS H 020

JCMAS H 020:2007 is a standard for testing the fuel consumption of the hydraulic excavators. The standard provides test cycles for digging and loading, leveling, traveling, and idling. All movements, except idling, are operated on maximum speed, such that at least one of the actuators moves on full speed. The height and depth limits are determined by the excavator size, which depends on the bucket volume, and the duty cycles of the smallest excavator (bucket volume 0.28 m^3) are described in this section.

The digging and loading cycle is illustrated in Figure 4, and it is performed the following way. The digging depth is 1.0 m (the bottom line in the figure), and the loading height is 2.0 m (the top line in the figure). In the starting position, the bucket is reached as far forward as possible, and the bucket is held 0.1 m above the ground (the middle line in the figure). Next, the arm is pulled towards the excavator body, until the arm is vertical to the ground. After that, a scooping movement is performed with the bucket, until the bucket face is horizontal. Both boom and swing are then operated to bring the bucket 90 degrees sideways and just above the loading height, where the bucket is unloaded by turning it until the bucket tooth are aligned with arm. Finally, the swing, boom and arm are returned back to their initial positions. For a complete test, this pattern is repeated five times. The shortest and longest cases are rejected, and remaining three cases are used to calculate the fuel consumption.

Figure 4: Digging and loading cycle

Leveling motion is done by actuating only boom and arm, and the leveling length is 2.5 m. This cycle is visualized in Figure 5. The movement is started from the same initial position as the digging cycle: bucket reached full forward and bucket tooth 0.1 m above the ground. Next, the boom is lifted while the arm is pulled towards the driver, until the desired leveling length is attained. After the movement, the boom and arm are returned back to the initial position. This pattern is repeated ten times for a complete test, and the test is done five times, longest and shortest of which are again discarded.

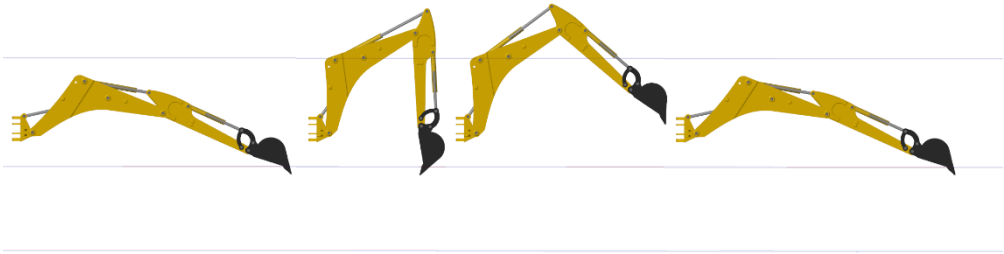

Figure 5: Leveling cycle

The traveling motion test is done by driving on full throttle on low speed (turtle) mode, for at least 25 m on concrete or other hard surface, without turning. For one test, the machine is driven forwards and backwards, one time each, and the time and fuel consumption is measured. The last test, idling, is done by simply letting the machine idle for 600 seconds, and measuring the fuel consumption.

The standard has some considerable limitations. First, the duty cycles do not involve any contact between the bucket and the earth. Therefore, they are not optimal for evaluating the efficiencies in real work, but rather to comparing the results between different machines, tested with the similar duty cycles. Second, the standard is addressed for excavators with bucket size greater than 0.25 m^3, but the bucket of the JCB micro excavator is only 0.022 m^3 – less than one tenth of the smallest excavator in the standard. The size of the excavator affects the reach, which makes is impossible to perfectly meet the requirements of the Japanese standard. However, keeping these limitations in mind, the standard may still be applied to produce comparable results of the efficiency of the excavator under investigation.

The standard is lately utilized in a simulation study (Ketonen & Linjama, 2017), in which the JCMAS truck loading and earth grading cycles were followed to avoid the modeling of contact with earth.

2.3.2 Other duty cycles

In (Zimmerman et al. 2007) a ‘typical digging cycle’ was used. This included digging a load of dirt, rotating, unloading the dirt, and returning back to starting position, quite similarly as in the JCMAS standard. The duty cycle involved multi-actuator movement,

aiming to reveal the phases of high inefficiency of the LS system. An improvement to the JCMAS standard was the use of artificial external load, consisting solely of a time-dependent load mass, which was applied to the bucket during the time it would be filled with soil. The force required to break into the earth was still ignored.

(Hippalgaonkar & Ivantysynova 2013) used two different truck loading cycles, to test the excavator with direct controlled actuators. The *expert cycle* starts by digging loose soil from the bottom of a pit, and unloading the soil into the bed of a truck at 6 ft (1.83 meters) after 90 degrees cabinet swing. After that, the machine returns to the digging position, and repeats the cycle, total time of which is 9.2 s. In the *novice cycle*, the soil is dumped on the ground level and the swing angle is only 40 degrees. As the cycle names suggest, the expert cycle includes multi-actuator movements, and it is considered to represent the maximal power demand from the hydraulics. Novice cycle, in turn, is mostly operated with one actuator at a time, which leads to longer cycle time and lower average power demand.

3. EL-ZON JCB MICRO EXCAVATOR

The EL-Zon project researches the application of decentralized DDH units to create competitive advantages for the companies related to the project. The challenges include, among others, combination of electric and hydraulic technologies, sensor-less positioning, and evaluation of possibilities for energy regeneration.

A mine loader and a mini excavator are chose as technology demonstrators of the project. The study cases of the EL-Zon project are not limited to mobile applications, but also a stationary application is developed. The DDH actuators of the mining loader are currently in use and being research, and the application into excavator is in preparation.

3.1 Background

In this project, a JCB 8008 CTS micro excavator is took as the test subject. The machine selection criteria are laid out in a thesis (Kiviranta 2009). The excavator size was limited by maneuverability, and limited storage and laboratory space. However, six degrees of freedom were desired in order to provide enough challenge for the automation development. Easy access to all components, fair price, and availability were also considered as JCB's advantage.

The excavator has been modified to serve research of software development by instrumenting it with orientation sensors and electrically controlled directional valves (Kiviranta, 2009). These orientation sensors are disassembled by today, but the directional valves, namely Danfoss PVG32, are currently in use.

The original 14 kW diesel engine of the excavator was subsequently replaced with a 10 kW electrical motor. The motor is driven by a Sevcon Gen4 motor controller, which is designed to control 3-phase-AC induction and permanent magnet motors (Sevcon). Besides the apparent reduction in the emissions, the electrification resulted in lower noise level, while maintaining approximately the original performance. However, the operational time of the excavator was reduced to two hours, even though the 60 Ah battery pack was considered high grade. Compared to the operation time of the diesel engine version, 8 hours with 15 l of fuel, the usability of the electrified version was considerably weaker. (Maharjan et al. 2014).

To address this drawback, a start-stop system was developed (Hassi et al. 2016). The implementation features a microcontroller and a mechanical limit switch, which activates when a valve is actuated. The microcontroller then starts the electric motor, and stops it when the system is idle for a predetermined period of time. The energy saving applies only to the idling period, and thus depends on the working cycle. Hassi et al. estimated

that the excavator is on idle at least 50% of the time it is used, which results in 32% reduction in energy consumption.

The excavator is currently powered by a battery pack of six 12 V batteries connected in a series, producing a 72 V voltage.

3.2 Conventional hydraulic system

For clarity, the *conventional* hydraulic system refers to the current setup, which is powered by the electric motor, and controlled with electrical valves. In contrast, the factory-made system, with diesel engine, and manually controlled directional valves, is referred to as *original system*.

The current, modified hydraulic system of the excavator is illustrated in Figure 6. The battery pack (1) is used to power the motor controller (2) and the electric motor (3). Two parallel fixed volume gear pumps (4), Parker PGP511, are connected to the motor shaft via a coupling. In the original hydraulic circuit, the volume flows of the two pumps were directed separately for different directional valve groups to ensure the flow supply in case of simultaneous actuator movements. In the modified system, the volume flows of both pumps are directed into a junction block (5). The first and dominant pressure relief valve is also located in this block.

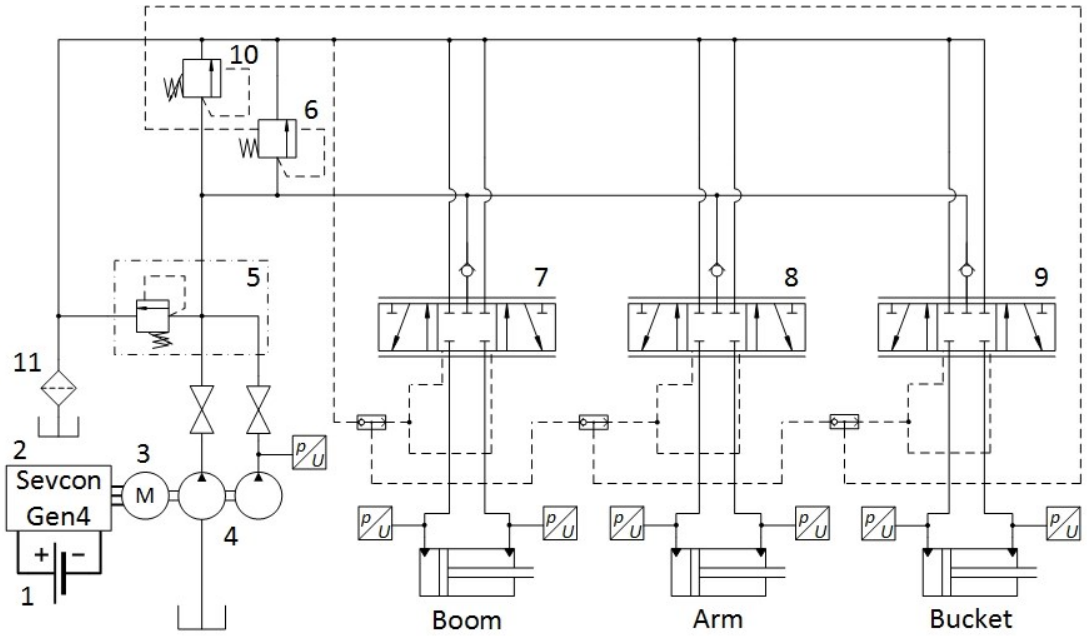

Figure 6: Simplified hydraulic schematic of the conventional system of the excavator

After the pressure relief valve block, the flow is directed to the inlet port of Danfoss PVG 32 directional valve group. The pressure adjustment spool (6) is constantly operating to adjust the pressure level at the directional valves (7, 8, 9), based on the pressure signal acquired from the valve ports. The functionality of directional valves is described in detail

in section 4.1.4. The pressure relief valve (10), of the directional valve group, is normally closed. From the directional valves, the oil flows through hoses into the cylinder chambers, and returns into the tank. The tank port of the directional valve is connected to the tank with a hose, and the oil flow is led to the tank trough a filter (11).

The inner diameter of the hoses between the directional valves and cylinders is ¼" (6 mm) and the hose between pumps and the valves 3/8" (9.5 mm). The hose between the valve block and tank has an inner diameter of ½" (12.7 mm).

3.2.1 Directional valves

The control valve is Sauer Danfoss PVG 32. Detailed reasoning behind the valve selection is presented in (Kiviranta 2009). The valve has separate spools for each actuator, although only boom, arm and bucket spools, spool numbers 3, 4 and 5 in the valve block, are included in the study. The valve set is installed parallel to original set, and the manually operated valves are used to activate either one of the directional valve sets.

A PVG 32 proportional valve group consists of three main modules: pump side module (PVP), basic modules (PVB), and actuation modules. The PVP connects to the pump and tank ports, and it has different functions depending on the application. In this valve group, the PVP is an open center version, which is to be used with fixed displacement pumps. The manufacturer part number is 157B5110, and the operation is explained in detail in (Danfoss, 2016). The system pressure is adjusted by a pressure adjustment spool (6), which, when the control spools (7, 8, 9) are in neutral, is fully open and lets the oil flow to the tank. When any of the control spools are actuated, the load-sensing channel is pressurized up to the highest load pressure, which causes the pressure adjustment spool to limit the flow to maintain a constant pressure difference between the load and system pressure. The hydraulic schematic of the PVP module, provided by the manufacturer, is shown in Figure 7.

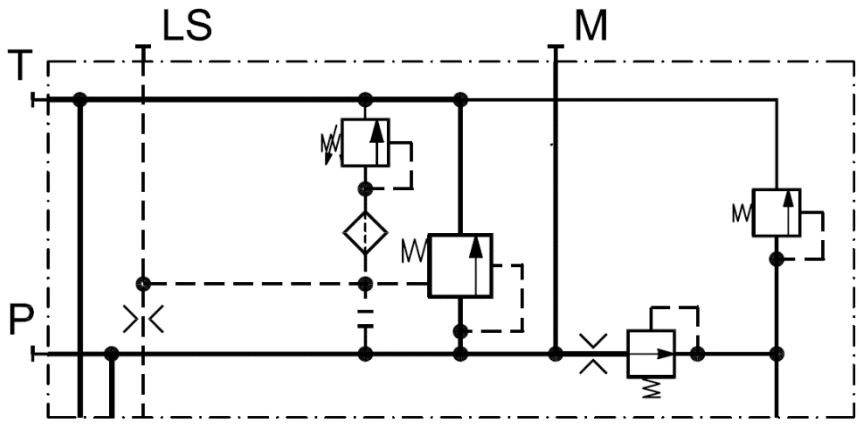

Figure 7: Pump side module 157B5110 (Danfoss, 2016)

The PVP module includes also the pressure relief valve (PRV). In actual system there are two PRV's, one at the junction point where the volume flows of two pumps meet, and another one at the valve block. The nominal set point of the valve block PRV is 180 bars, but as the other PRV opens near 130 bars, the valve block PRV stays closed at all times.

The basic modules, or PVB's, each include control spool for one actuator. Manufacturer part number is 157B6100 for the PVB module and 7005 for the spool. The hydraulic schematic for a single PVB is shown in the Figure 8 on the left and for the spool in Figure 8 on the right. The logic of the load-sensing circuit is that when the spool is actuated, the load-sensing channel connects to the respective port. A shuttle valve circuit selects the highest load of all actuated PVB's, and passes it forward to the PVP module. The pressure channel of the PVB is also equipped with check valve to prevent return oil flow.

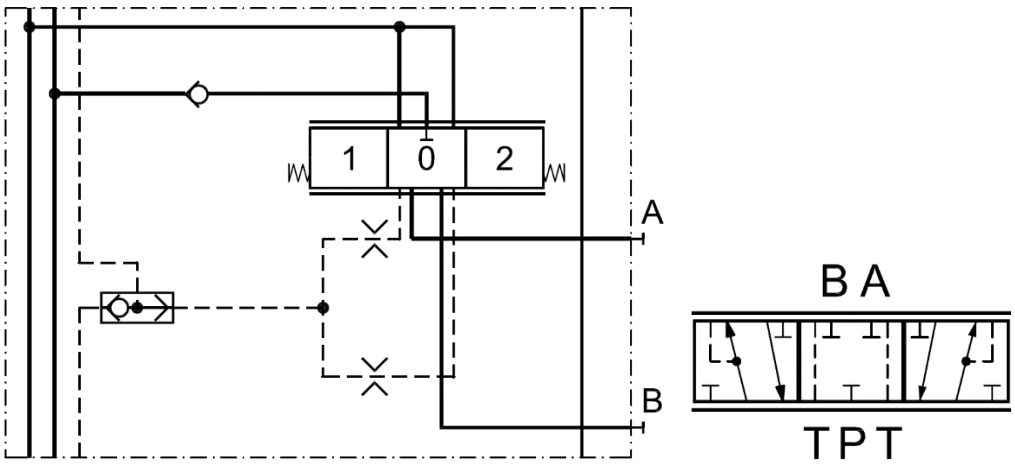

Figure 8: left: Basic module 157B6100; right: spool 7005 (Danfoss, 2016)

3.3 Instrumentation

The measurement, control, and data acquisition system is described in detail in Appendix A. Only a short overall explanation is given in this section. Physical measurements on the excavator provide data for parameterization and verification of the simulation model. The excavator is fitted with pressure sensors in all cylinder ports and in the pump outlet port, and position sensors at the cylinder rods. The measurement signals are collected and recorded at a target-pc. A simple position feedback controller is established to move the front hoe in a safe and controlled manner. The topology of the measurement, control and data-acquisition system is illustrated in Figure 9. Communication channels are visualized as lines, with the text pointing out the communication protocol. Boxes with solid line represent hardware and boxes with dotted line are software.

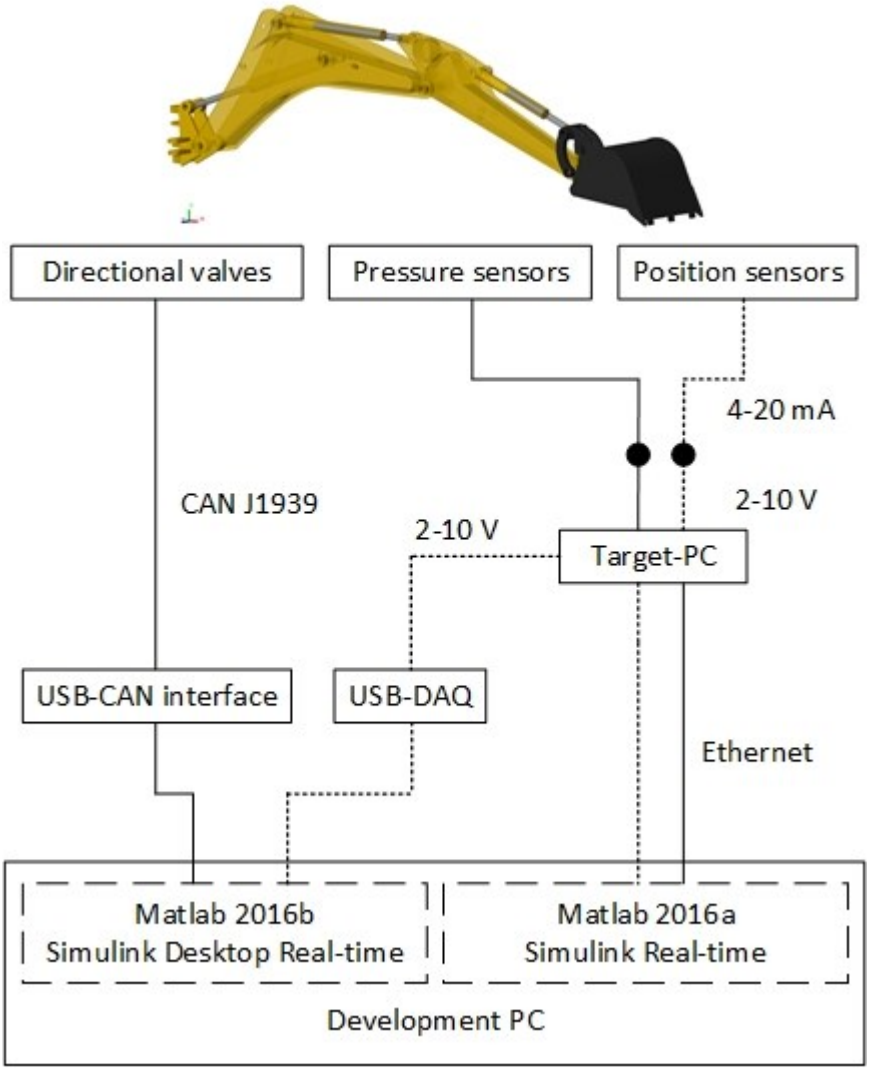

Figure 9: Measurement, control, and data acquisition system of the excavator

Simulink Real-Time -toolkit enables creating real-time applications from Simulink models. They run on a dedicated target computer, which is connected to the physical system via analog I/O ports. In this project, the real-time setup is used to collect the measurement data from pressure transducers and position sensors.

The Danfoss PVG 32 valves are equipped with electro-hydraulic control modules PVED-CC. Communication between valves and computer uses CAN J1939 protocol. Simulink provides blocks necessary to communicate with the bus, and, together with the real-time kernel, enables driving the model in real-time, without having to use an additional target pc. Thus, the user interface is divided in two separate systems: the target-pc system and the desktop real-time system.

4. SIMULATION MODEL

A simulation model is created in Matlab Simulink environment to study the dynamic behavior of the excavator. The rationale and equations used in the model are presented in the following sections, to ensure the repeatability of the study results, and also to serve as documentation for other users of the model. As in all simulation, it is necessary to recognize the limitations of the model, as it takes into account only the phenomena that are built into it.

The emphasis of this work is in modeling the conventional system, meaning the system with centralized pump and a valve control, presented in Figure 6. It is noteworthy, that the term 'LS system' is commonly used to describe a system with a variable-displacement pump. The conventional system of the excavator, however, has a fixed-displacement pump with constant rotational speed. It senses the load pressure, and adjusts the system pressure accordingly, by directing the excess volume into the tank, via the pressure adjustment valve.

The DDH actuator is modelled earlier by (Järf 2016), and as the model is verified and well documented, it is used as is, without detailed explanation. First, all the submodels, or components, of the model are explained in detail. After that, the verification results are presented. Then, a brief explanation is given, concerning the combination of DDH actuators with the rest of the excavator model.

4.1 Conventional model

This work is focused in the hydro-mechanical system of the excavator front hoe. The simulation model includes the hydraulic pump, directional valve group, auxiliary valves, hydraulic cylinders, the mechanical model of the front hoe, and the connecting hoses. The electric motor and the motor controller are assumed ideal, with 100% efficiency and constant rotational speed. Following sub-sections will introduce utilized equations and Simulink realizations for the modelled components.

4.1.1 Volume model

The volume model is one of the basic components in modelling dynamics of the hydraulic systems. Compressibility derives from transformation of components and fluid under pressure. As the pressure increases, the volume of the fluid decreases. At the same time the hoses, pipes and different chambers expand and their volume is increased. This causes inaccuracy and vibration to the actuator movement, which is harmful, especially in applications, in which the exact positioning is relevant. The compressibility of a hydraulic system can be expressed as a volume differential:

$$\Delta \boldsymbol{V} = \frac{\mathbf{1}}{\boldsymbol{B_{eff}}} \cdot \boldsymbol{V_t} \cdot \Delta \boldsymbol{p} \qquad \textit{(8)}$$

$$\frac{\mathbf{1}}{\boldsymbol{B_{eff}}} = \frac{\mathbf{1}}{\boldsymbol{B_f}} + \sum_{\boldsymbol{i=1}}^{\boldsymbol{n}} \left(\frac{\boldsymbol{V_{ci}}}{\boldsymbol{V_t}} \cdot \frac{\mathbf{1}}{\boldsymbol{B_{ci}}} \right) + \frac{\boldsymbol{V_a}}{\boldsymbol{V_t}} \cdot \frac{\mathbf{1}}{\boldsymbol{B_a}} \qquad \textit{(9)}$$

Notation	Explanation	Unit
ΔV	volume differential	m^3
B_{eff}	effective bulk modulus	Pa
V_t	total volume of the system	m^3
Δp	pressure differential	Pa
B_f	bulk modulus of the fluid	Pa
n	number of components	-
V_c	volume of a component	m^3
B_c	bulk modulus of a component	Pa
V_a	volume of insoluble air	m^3
B_a	bulk modulus of insoluble air	Pa

The change in fluid volume may be due to change in component volume, which is the case in, for example, a hydraulic cylinder. Nevertheless, the same effect is observed, when a fluid volume is introduced to (or taken away from) a fixed-size container. A typical case is a volumetric flow entering a hydraulic hose, which is already filled with oil. As the volume increases, according to the equation 8, also the pressure increases. This causes a transformation (volume increase) in the hose.

If entering and leaving volumetric flows are marked as a net volume flow $\sum Q$, and combined into equation 8, a state equation of the volume may be formed:

$$\frac{\boldsymbol{dp}}{\boldsymbol{dt}} = \frac{\boldsymbol{B_{eff}}}{\boldsymbol{V_t}} \cdot \left(\sum \boldsymbol{Q} - \frac{\boldsymbol{dV}}{\boldsymbol{dt}} \right) \qquad \textit{(10)}$$

In the Simulink model, the fluid volumes are modeled separately, instead of lumping them together. Now the effective bulk modulus only consists of bulk moduli within particular component: fluid and the component itself. The pressure is assumed equal across the whole volume. Thus the length of the volume is assumed to be short compared to the

speed of sound in oil (approximately 1400 m/s), and there must not be any significant pressure losses within the volume.

The volume of insoluble air, typically 0.1-5% of the fluid volume, may have a dramatic effect on the system compressibility. The effective bulk modulus of the system drops rapidly in near-zero pressure. (Kauranne et al 2008). This causes the pressure remain close to atmospheric pressure even when the oil flow into the volume is positive. The bulk modulus of insoluble air is solved from equation:

$$\boldsymbol{B_a = 1.4 \cdot p}\,, \qquad \textit{(11)}$$

where p is the variable system pressure. The effective bulk modulus is then calculated with equation 9. The effect of free air is observable in A-chambers of boom and arm cylinders, and the free air model is implemented in order to make the simulation results match the measurement data. The estimated amount of free air in the boom cylinder is 0.8% and in the arm cylinder 0.11%.

4.1.2 Orifice model

Another frequently used submodel is the orifice model, which is used to calculate a volumetric flow, caused by a pressure difference over a flow path. Fluid flow can be laminar, turbulent, or a combination of these. The nature of the flow depends on the flow speed, kinematic viscosity and a hydraulic diameter of the flow path. These parameters form a so-called Reynolds number in the following way (Kauranne et al. 2008):

$$\boldsymbol{Re = \frac{v \cdot D_H}{\nu}} \qquad \textit{(12)}$$

Notation	Explanation	Unit
Re	Reynolds number	-
v	flow speed	m/s
D_H	hydraulic diameter of the flow path	m
ν	kinematic viscosity	m^2/s

For different flow paths, there are experimentally found critical Reynolds numbers, at which the flow is expected to change from laminar into turbulent. For example, in round, smooth piping, the critical Reynolds number is around 2000-2300 (Kauranne et al. 2008).

In hydraulic system modeling, the flow under greatest concern is typically turbulent. In (Bak & Hansen) the flow is assumbed turbulent. However, as pointed out by (Ellman &

Piche 1996), the transition over zero pressure has caused problems with ODE solvers, when using conventional turbulent flow equation. They have proposed an equation, in which a polynomial laminar flow formula is used, when the pressure difference is below the transition pressure. This replaces an infinite derivative in zero-pressure with a finite physically realistic value. The formula proposed is:

$$q(p) = \begin{cases} C \cdot A \cdot \sqrt{\dfrac{2p}{\rho}} & (p > p_{tr}) \\ \dfrac{3\,A\,\nu\,Re_{tr}}{4\,D}\left(\dfrac{p}{P_{tr}}\right)\left(3 - \dfrac{p}{p_{tr}}\right) & (0 \le p \le p_{tr}) \end{cases} \qquad (13)$$

Notation	Explanation	Unit
Re_{tr}	transition Reynolds number	-
C	flow coefficient	-
A	orifice area	m^2
p	pressure (difference over orifice)	Pa
p_{tr}	transition pressure	Pa
D	orifice diameter	m
ρ	fluid density	kg/m^3

Flow coefficient C, orifice diameter D and fluid density ρ are assumed constant and included to a new parameter K_V, which is defined as:

$$K_V = CA\sqrt{\frac{2}{\rho}} \quad where \quad C = \frac{q}{A}\sqrt{\frac{\rho}{2p}} \quad \rightarrow \quad K_V = \frac{q}{\sqrt{p}} \qquad (14)$$

The constant part of the equation for laminar flow can be expressed with a single constant C_{lam}:

$$C_{lam} = \frac{3\,A\,\nu\,Re_{tr}\sqrt{p_{tr}}}{2\,D}, \qquad q = \frac{C_{lam}\,p}{2\sqrt{p_{tr}}}\left(3 - \frac{p}{p_{tr}}\right) \qquad (15)$$

At the transition pressure $p = p_{tr}$ it is discovered that

$$q_{lam}(p_{tr}) = q_{turb}(p_{tr}) \quad \rightarrow \quad \frac{C_{lam}\, p}{2\sqrt{p_{tr}}}\left(3 - \frac{p}{p_{tr}}\right) = K_V \cdot p \quad \rightarrow \quad C_{lam} = K_V \tag{16}$$

Possible change in the flow direction is taken into account by changing the pressure difference *p* into absolute value, marking pressure difference as subtraction of pressure before and after the orifice, and adding a sign-function. The original piecewise equation can now be written as:

$$q(P) = \begin{cases} K_V\, sgn(p_1 - p_2)\sqrt{|p_1 - p_2|} & (|p_1 - p_2| > p_{tr}) \\ \dfrac{K_V(p_1 - p_2)}{2\sqrt{p_{tr}}}\left(3 - \dfrac{|p_1 - p_2|}{p_{tr}}\right) & (|p_1 - p_2| \le p_{tr}) \end{cases} \tag{17}$$

Figure 10 illustrates the realization of equation 17 in Matlab Simulink environment. The orifice subsystem is later utilized in hose and valve models.

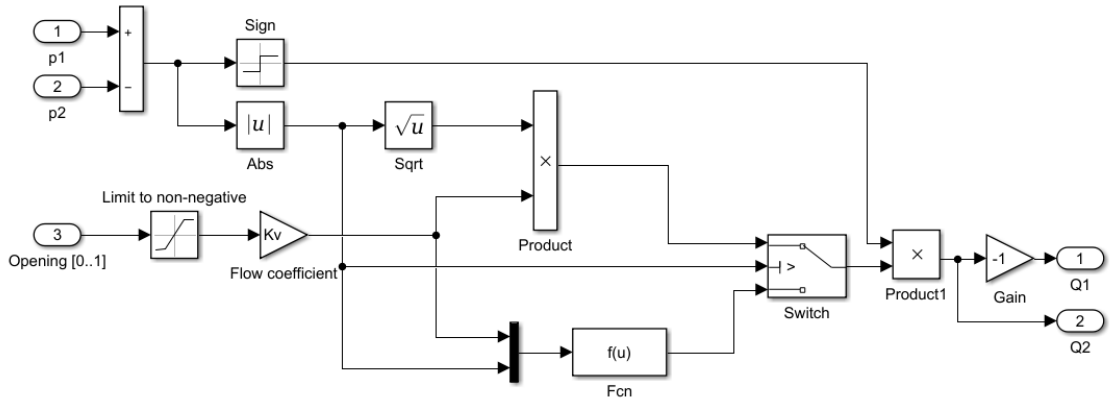

Figure 10: Orifice model

4.1.3 Hose model

In the hydraulic system, hoses are utilized to transmit hydraulic power between virtually all components. The pressure drops of the hoses are expected to be significant, because the hoses are relatively narrow (6.0-12.7 mm) in diameter, and most of them are long and bent. However, determining the pressure drop experimentally, for every component in the system, is not possible within the scope of this work, so they must be estimated by mathematical formulas found in literature. The model used to estimate the flow losses is based on the paper (Avci & Karagoz 2009). For laminar flow, the pressure drop Δp, caused by pipe friction, can be written as (Kauranne et al. 2008):

$$\Delta \boldsymbol{p} = \boldsymbol{\lambda} \cdot \frac{\boldsymbol{l}}{\boldsymbol{d}} \cdot \frac{\boldsymbol{\rho}}{\boldsymbol{2}} \cdot \boldsymbol{v^2} \qquad \textit{(18)}$$

Notation	Explanation	Unit
Δp	pressure drop	Pa
λ	friction factor	-
l	pipe length	m
d	pipe inner diameter	m

The friction factor λ is relative to Reynolds number *Re*. For laminar flow it is

$$\boldsymbol{\lambda_{laminar}} = \frac{\boldsymbol{64}}{\boldsymbol{Re}} \qquad \textit{(19)}$$

Friction factor can also be determined for non-laminar flow. This lets us use the laminar flow equation for all flow types. The friction factor for turbulent flow is (Avci & Karagoz 2009):

$$\boldsymbol{\lambda_{turbulent}} = \frac{\boldsymbol{6.4}}{\left(\boldsymbol{ln(Re)} - \boldsymbol{ln}\left(\boldsymbol{1 + 0.01\, Re\, \varepsilon\left(1 + 10\sqrt{\varepsilon}\right)}\right)\right)^{\boldsymbol{2.4}}}, \qquad \textit{(20)}$$

where ε is the relative roughness of the pipe, $0 \leq \varepsilon \leq 0.05$.

In the transition phase between laminar and turbulent flow, the friction factor is modeled with a simple continuous function, which is also continuously differentiable. The accordant friction factor is selected based on the Reynolds number: the laminar flow factor is used for Reynolds numbers below 2300, transition flow factor for $2300 \leq Re \leq 4000$, and for the Reynolds number greater than 4000, the flow is assumed to be fully turbulent, and the turbulent flow friction factor is used.

In addition to pipe friction, there are flow losses in the system, which are related to change of speed or direction of the flow. These losses are present in joints and bends, for example. (Kauranne et al. 2008). These losses can be calculated from equation 21:

$$\Delta \boldsymbol{p} = \boldsymbol{\zeta} \cdot \frac{\boldsymbol{\rho}}{\boldsymbol{2}} \cdot \boldsymbol{v^2}, \qquad \textit{(21)}$$

where ζ is the unitless friction factor. Kauranne et al. have listed values for the factor ζ, and the ones used in this work are collected in Table 1.

Table 1: Factor values for pipe friction

Component	Friction factor (ζ)
Straight pipe joint	0.5
Angle joint	1.0
Bent pipe	0.4
Pipeline branch	1.0
Valves	3.0-6.0

For example, the pipeline between the bucket cylinder and the valve block consists of a 90-degree angle joint, two straight pipe joints, 3.8 meters of hydraulic hose, and one bent pipe, which results in friction factor ζ value 2.4.

A complete hose model consists of the pipe friction, orifice, and volume models. The block diagram of the model is shown in Figure 11.

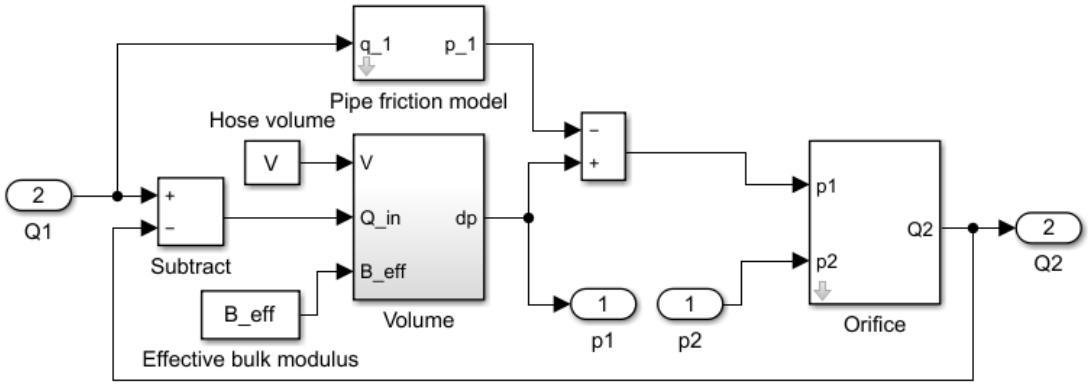

Figure 11: Hose model

The model is masked, and parameters, such as hose inner diameter and length, are given in the mask. Variable inputs for the hose model are incoming flow, and pressure after the hose. The model outputs are outgoing flow, and the pressure before the hose.

4.1.4 Proportional valve model

The functionality of the directional valve is presented in section 3.2.1. The main modules are the pump side module (PVP), which includes pressure adjustment spool and pressure relief valve, and the basic modules (PVB), which include directional spools. The pressure

adjustment spool is modeled with a lookup table, result of which corresponds the graph given by the manufacturer, although some adjustments are applied to make the simulation model match the measured data. A rate limit block is added to limit the transition speed of the spool, and the flow is saturated to minimum of 0 l/min, and maximum of 140 l/min.

The PRV is modeled based on the manufacturer data. The Simulink model is virtually the same as of the pressure adjustment spool, only with different parameters. The specified set point for the valve block PRV is 180 bars. However, the system pressure is, based on the measurements, limited to 120-130 bar. Thus, the pressure limit of the valve block is never reached, and only the first PRV activates when the pressure rises up to the limit. The behavior of the PRV is visible in Figure 12, in which the measured and simulated system pressure are plotted together.

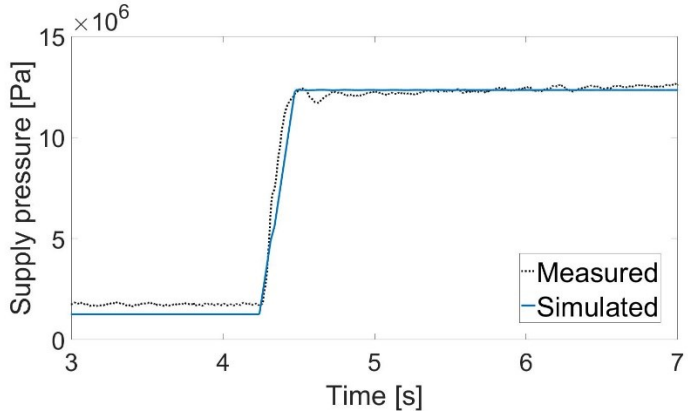

Figure 12: Pressure relief valve opening

The PVB, or directional spool, model is controlled with a spool position command *u,* and it outputs the flow for each valve port (P, A, B, T). It also compares the load pressure of the active port against the loads on other spools, and passes forward the highest pressure. The Simulink model of a PVB module is presented in Figure 13.

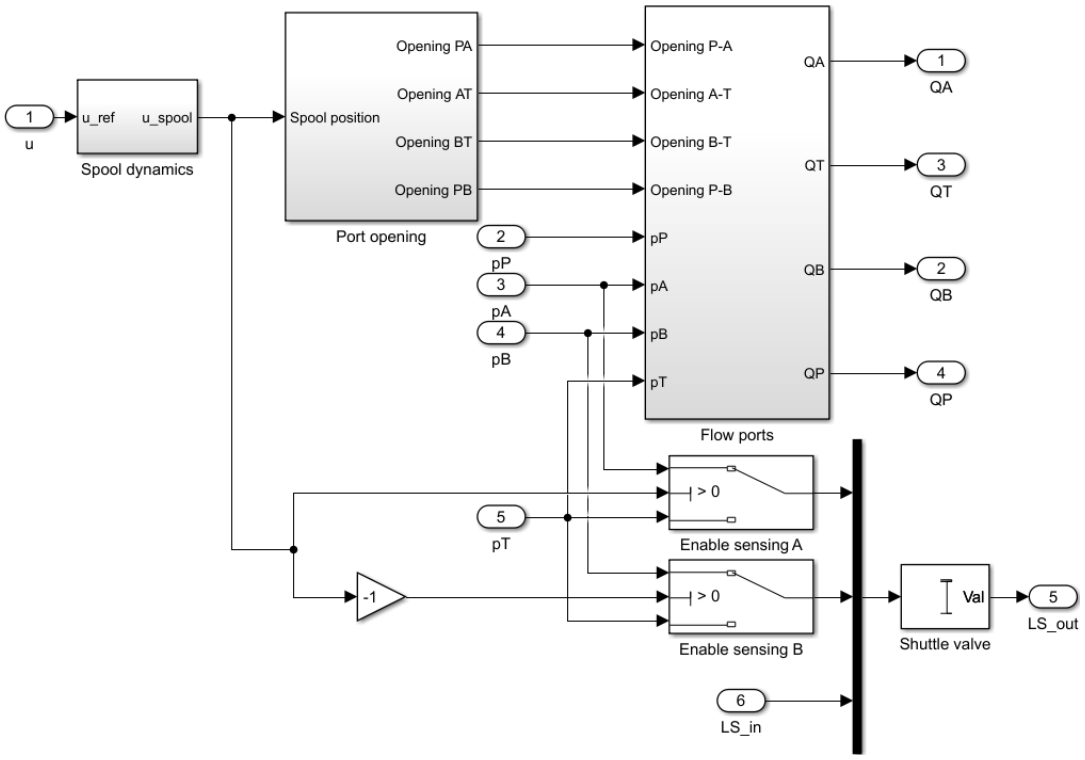

Figure 13: Simulink model of a PVB module

The spools response to the command signal is determined by spool dynamics, which consists of a transfer function and a saturation block. The transfer function is from the work of (Bak & Hansen), who studied the dynamic behavior of a PVG 32 valve. It must be noted, that this valve has different spool size and different components, so the transfer function parameters serve only as an estimation of the actual spool dynamics. However, it is not possible or even desired to model our valve in such a detail, and the estimation is sufficient for this purpose. The second-order transfer function is written

$$\boldsymbol{u_{spool} = \frac{1}{\frac{s^2}{\omega_n^2} + 2 \cdot \zeta_d \cdot \frac{s}{\omega_n} + 1} \cdot u_{ref}} \qquad \textit{(22)}$$

Notation	Explanation	Unit
u_{spool}	Spool position	-
u_{ref}	Reference signal	-
ω_n	Natural frequency	Hz
ζ_d	Damping ratio	-

The spool position is then converted into the relative opening of each control edge of the spool. A linear opening would result in satisfactory estimation, but since measurement

data is available, the port opening is tuned for more realistic behavior in partially open valve states. The port openings, as a function of spool position, are shown in Figure 14, which also points out the symmetry of flow in both directions.

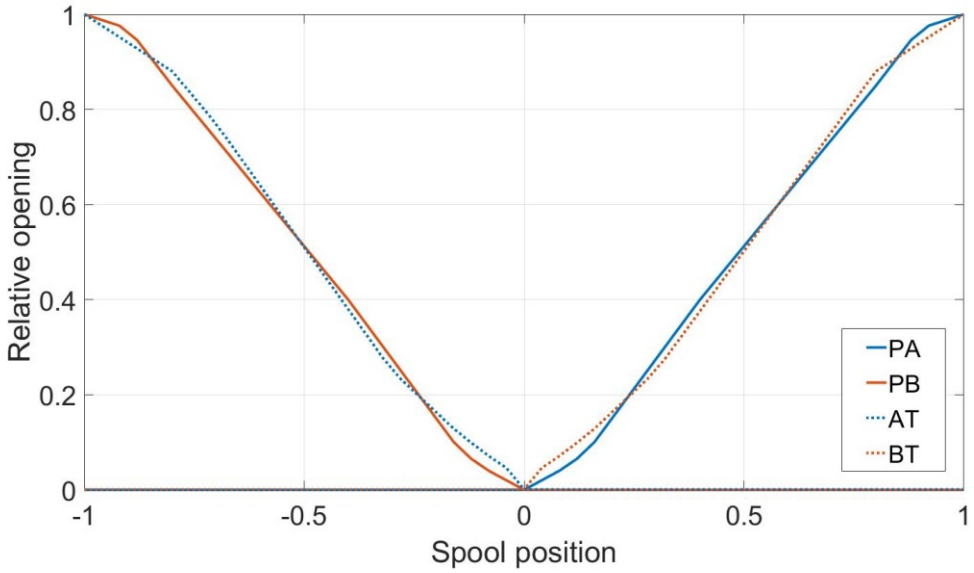

Figure 14: Relative opening for each valve port

The opening is modeled with four lookup tables, one for each control edge. The spool leakage is also modeled in this point, by leaving the tank edges partially ($8e^{-4}/1$) open, when otherwise in closed position. This results in leakage flow (and actuator drift) matching the measured data.

Oil flow through the ports is calculated with four separate orifice blocks, as described in section 4.1.2. These blocks utilize the opening value as an input, and calculate a volumetric flow based on the pressure difference over the spool. The flow coefficient K_v is calculated for each valve port from equation:

$$\boldsymbol{K_V = \frac{q_{nom}}{\sqrt{p_{nom}}}}, \qquad \textit{(23)}$$

where q_{nom} is the nominal flow [m^3/s], and p_{nom} is the nominal pressure differential [Pa]. Based on the measurement data, the nominal flows of the spools are in the range of 5.3-5.6 l/min at the pressure difference of 10 bar, which corresponds with the nominal spool size, 5 l, given by the manufacturer. All the parameters are presented also in Appendix C.

4.1.5 Cylinder model

The function of a cylinder model is to transform the introduced volumetric flow first into chamber pressures and then into output force. The cylinder model itself does not actually

produce any movement, and therefore it needs to be connected into a mechanical model, from which it may acquire the position and velocity inputs. The movement of the piston is limited by end cushion subsystem, which produces a force required to prevent the piston from extruding out of the cylinder ends. The output force of the cylinder is also affected by the friction, which is modeled with another subsystem, respectively. The subsystems of the cylinder model are presented in Figure 15.

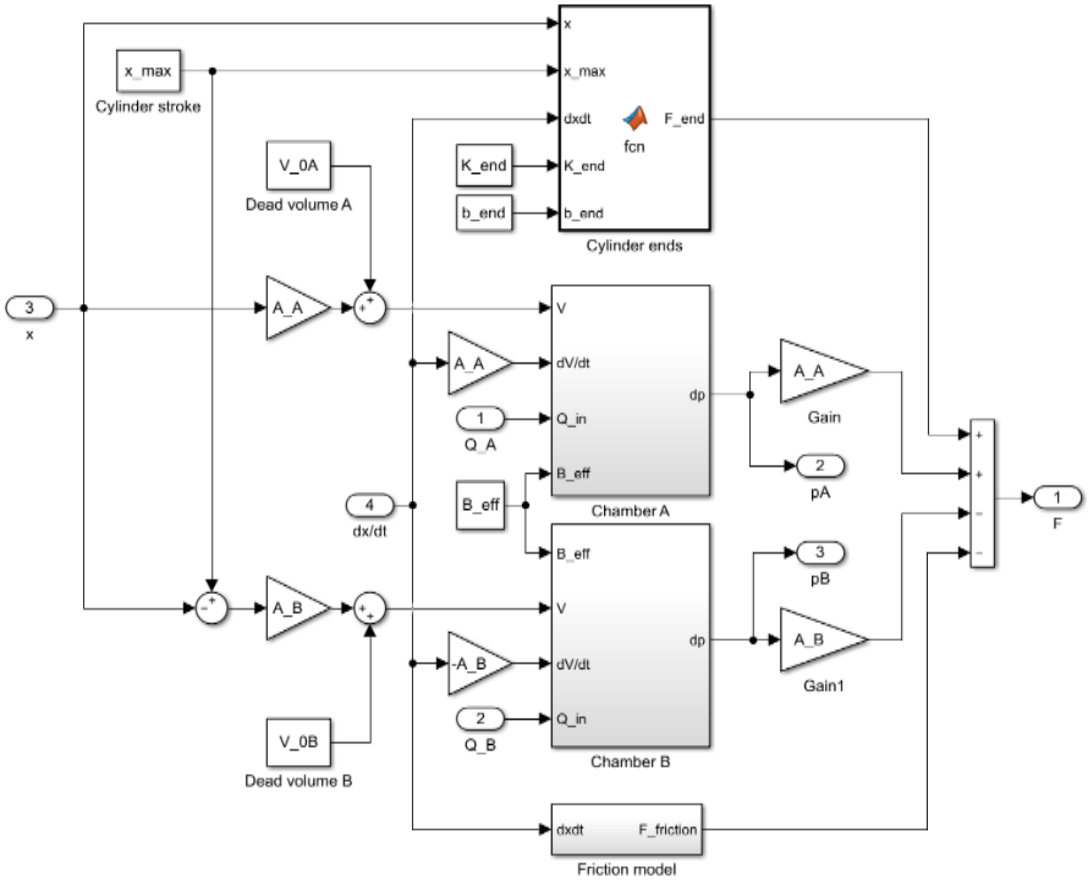

Figure 15: Subsystems of the cylinder model

The chamber subsystem is based on the previously introduced volume model. The volume *V* and the volume differential *dV/dt* are calculated from the piston areas, and position and velocity, which are acquired from any mechanical model attached downstream of the cylinder model. The introduced flow *Q_in* is the output flow of respective valve port. The output force is then the product of chamber pressure and the piston area on that side.

Cylinder end cushions are modeled as stiff springs, with such a spring constant, which prevents the piston from extruding out of the cylinder end. In the end position, the chamber volume is close to zero. Zero volume will cause the simulation to crash due to a division function in the volume model. To prevent this, also the dead volume, which is the amount of fluid that is left in the chamber in zero-position, must be included in the model.

Cylinder friction consists of forces between surfaces of the cylinder and the seals, which includes seals of piston and piston rod. Having an accurate friction model is vital for two reasons. First, it is needed to make a reliable simulation model. In a conventional, valve controlled system, the cylinder frictions were responsible for relatively little part of the total losses. In direct-driven hydraulics, this part is expected to be significantly more remarkable, and, thus, under greater interest. Secondly, as the EL-Zon project aims to sensorless control of the actuators, estimating the friction forces, and thus the output force, becomes necessary.

Friction behavior is known to vary depending on multiple variables, such as properties of the contacting surfaces, their relative velocity, and amount and quality of lubrication. The static friction, appearing in near-zero velocities, is typically greater than the dynamic friction at low velocities. As the velocity increases, viscous friction of the lubricating film starts to increase, but the velocity dependency is usually non-linear. (Olsson et al. 1998). The fact that the friction is larger at rest that during movement, causes also the stick-slip motion, which can be observed as jerky movement of a cylinder at low speed and/or low pressure (Kauranne et al. 2008). Before the cylinder force exceeds the force required to win the static friction force, or break-away force, a minor displacement may be observed. This is called pre-sliding displacement, and during it the friction behaves like a spring. In addition, the break-away force varies depending on the rate of increase of the applied force. In varying velocity, there is a hysteresis in friction force. In other words, friction force for decreasing velocities is lower than for increasing velocities. The hysteresis increases as the rate of velocity changes increase. This behavior, also called frictional lag, is explained by just a time delay between velocity and friction force. (Canudas de Wit et al. 1995).

These phenomena make creation of an accurate friction model a challenging task. At the most simplified stage, so-called Coulomb friction model, the friction is modeled with just a step function, outputting a force with sign opposite to the velocity. The magnitude of force is proportional to the normal load only. Thus, the Coulomb model cannot exhibit changes in friction force in relation to velocity, nor specify the friction around zero velocity. In order to take the velocity into account, the model can be upgraded with a viscous friction coefficient or suitable exponential function. (Olsson et al. 1998).

In earlier work on EL-Zon project, (Järf 2016) exploited a dynamic friction model, proposed by (Canudas de Wit et al. 1995). The model takes into account most of the dynamic friction behavior, including Stribeck effect, hysteresis, sticktion, and varying break-away force. This model, also known as the LuGre model, is originally for modeling friction between two relationally sliding surfaces. In the model, the contact is thought as bristles, moving against each other. When applied to the cylinder friction, the bristles can easily be seen as representatives of the cylinder seals. The average deflection of the bristles is marked z, and its time derivative is modeled by:

$$\frac{dz}{dt} = v - \frac{\sigma_0 |v|}{g(v)} z \ , \tag{24}$$

where

$$g(v) = F_c + (F_s - F_c) e^{-\left(\frac{v}{v_s}\right)^2} \tag{25}$$

$$F_\mu = \sigma_0 z + \sigma_1 \dot{z} + \sigma_2 v \ . \tag{26}$$

Notation	Explanation	Unit
z	average deflection of bristles	m
v	relative velocity	m/s
v_s	Stribeck velocity	m/s
F_c	Coulomb friction	N
F_s	static friction	N
F_μ	friction force	N
σ_0	stiffness of bristles	N/m
σ_1	damping coefficient	Ns/m
σ_2	viscous friction coefficient	Ns/m

The initial values for friction coefficients are selected based on literature and previous studies, and improved according to the measurement data. Reference values for friction coefficients, found in the literature, are collected in Table 2.

However, as the friction force is low compared to pressure forces, the change in friction parameters cause little or no effect on the cylinder velocity. Therefore, friction parameters utilized in this work should be considered approximations only. Any pressure dependency of the friction is left outside this work, since the measurements do not clearly indicate such a behavior.

Table 2: Reference values for friction coefficients

Notation	(De Wit et al. 1995)	(Järf 2016)	(Hyvönen 2015)	Unit
v_s	0.001	0.0005	0.003-0.015	m/s
F_c	1	87.61	1000-5300	N
F_s	1.5	300	1700-5800	N
σ_0	$10e^5$	$3e^5$	$1.6e^6$-$5.8e^7$	N/m
σ_1	1000	547.72	5000	Ns/m
σ_2	0.4	41195	1700-5800	Ns/m

4.1.6 Hydraulic pump model

Two hydraulic pumps of the excavator are Parker PGP511 gear pumps, with a fixed volume of 6 ccm each. According to manufacturer data (Parker 2017), the PGP511 pump has a 12-tooth gear profile, and optimized flow metering to provide reduced pulsation and quiet operation. Therefore, the output flow is assumed "flat" and the possible fluctuation is not modeled. The theoretical flow is a product of volume and rotational speed:

$$q_{pump\_theor} = n_{pump} \cdot V_{pump} \qquad (27)$$

Notation	Explanation	Unit
q_{pump_theor}	Theoretical output flow of pump	m^3/s
n_{pump}	Pump shaft rotational speed	1/s
V_{pump}	Pump volume	m^3

However, real pumps are affected by leakage, caused by pressure difference between inlet and outlet ports. The initial model for volumetric efficiency of the pump is based on the flow/pressure curves provided by the manufacturer, and it is modeled with lookup tables, one table for each rotational speed. The performance data from the datasheet is visible in Figure 16. According to the curve, the leakage consists of a constant component and a pressure dependent component. The value of constant component is approximately 0.1 l/min, and it is reduced from the theoretical flow value regardless of the rotation speed or pressure. The pressure dependent factor is approximately $-3.1 \cdot 10^{-3}$ l/min/bar. This gives a linear correlation between volumetric losses and pressure difference over pump.

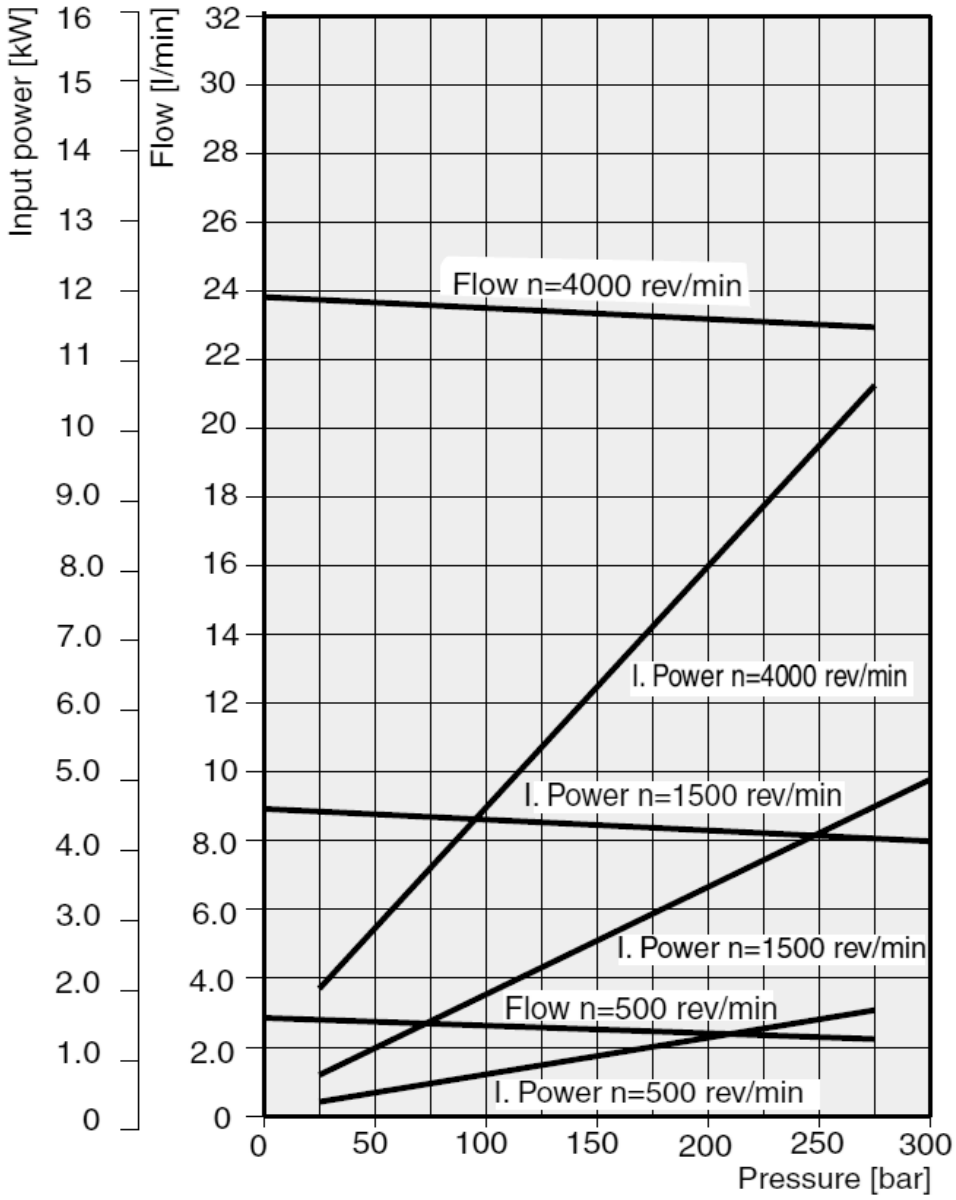

Figure 16: Performance data for Parker PGP 511 - 6.0 CC gear pump as provided by Parker Hannifin, 2017

The flow function is implemented with a *lookup table* block. The Simulink model of the pump subsystem is shown in Figure 17. The volumetric flows of the two pumps are connected shortly after the pump outlets, and, for simplicity, the hose after the pump is modeled as one volume. The pump output flow is summed with the (negative) flow consumed by the directional valves, pressure adjustment valve and pressure relief valve. Sum of all flows is utilized in a hose model to generate the supply pressure after the pump. The hose model is explained in more detail in section 4.1.3.

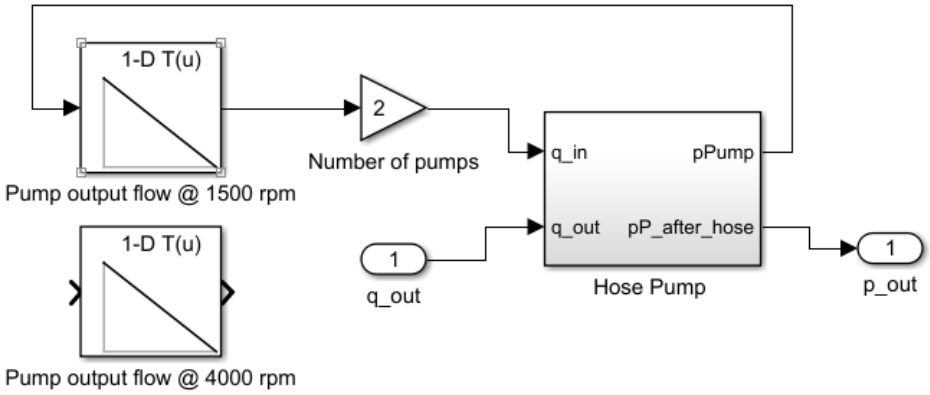

Figure 17: Hydraulic pump model

Lookup table for volumetric flow is connected manually, according to wanted rotational speed. A pressure rise is calculated in the hose model, based on incoming and leaving volumetric flows, and the pump model outputs the supply pressure.

4.1.7 Simscape Multibody model

In order to simulate the physical response of the mechanical system, a multibody model is created. Simscape Multibody is a toolbox, which provides blocks, such as solids, different joints, sensors and so on, to formulate and solve equations of motion (Mathworks 2017). A portion, representing the revolute joint connection between the kingpost and the boom, and the boom cylinder, is shown in Figure 18.

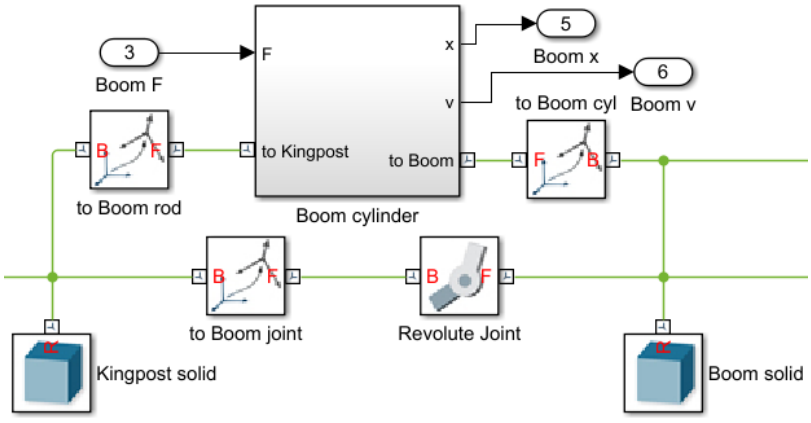

Figure 18: Connection between boom and kingpost

Positions of related joints are defined in separate matlab m-file, using Cartesian (x, y, z) coordinates. In some cases, it is necessary to rotate the coordinates. For example, a prismatic joint, in the cylinder model, allows movement only into the direction of z-axis. Therefore, the coordinates must be rotated accordingly. To achieve the best possible correlation between the model and actual mechanism, the dimensions of the solids are based on physical measurements. Additionally, the components are weighed and the mass centers are located. The measurement-based dimensions are presented in Appendix B.

However, the weight of the hydraulics attached to the front hoe, including hoses and the variable fluid volume, is unknown and must be estimated. Figure 19 depicts the 3D visualization of the front hoe model. The parts of the excavator are modeled in PTC Creo and exported to STEP files, which are utilized as sources for shape in solid blocks. This way the mass distribution is as close to the real as possible. In addition, a realistic visualization helps determining the duty cycle limits later in the study.

The interaction between hydraulics, which provides force as an output, takes place in the prismatic joints of each cylinder. The joint receives the force as an input, and computes the movement based on the mass properties of the multibody model. Position and velocity are acquired from the joint and can be used as such at the hydraulic model of the cylinder.

Figure 19: Multibody model of the front hoe

The mass distribution in the multibody model is finished by placing the connection pins in their actual locations and adding the weight of hydraulic hoses and fluid. The weight of the fluid inside a cylinder is assumed constant for simplicity, and it is calculated by multiplying the fluid volume of a mid-way extended cylinder by the density of the hydraulic fluid. As a result, the estimated oil weight for boom cylinder is 0.665 kg, arm cylinder 0.572 kg and bucket cylinder 0.406 kg, which are added to the cylinders. The weight of the hydraulic hoses is also assumed constant, and calculated by multiplying the length of the hoses with estimated weight per meter. The weight of the fluid is added to the value. The total estimated weight of the hoses filled with oil is 1.7 kg. Hoses are actually located close to the boom, and, therefore, this mass is lumped into the boom mass.

Modeling the detailed dynamic behavior of the mechanism would be a topic for another research. Therefore, following assumptions and simplifications have been made. All joints are ideal, and provide only certain degree of freedom. No friction acts on the joints.

Instead, it is taken into account in hydraulic cylinder model. Bodies are indefinitely rigid, no deflections or vibrations apply. In addition, the attachment point of the front hoe, the kingpost, is modeled with rigid connection to the world frame, whereas the actual excavator provides some degree of movement.

4.2 Model verification

First step in the model verification process is to compare simulated cylinder pressures against the measured pressures. In order to acquire the necessary measurement data, the excavator is controlled to move the arm cylinder from fully retracted position to fully extracted position and back on full speed. The arm valve flow signal (AVEF) is recorded and forwarded as an input for the spool position in the simulation model. Measured cylinder position, pressures in chambers A and B, and the system pressure at pump outlet port are plotted together with simulated values, and are shown in Figure 20.

Other actuators were driven in predetermined positions, to ensure corresponding inertial properties, but were not subject to control, to prevent any unwanted disturbance for the system pressure. Simulated pump and chamber pressures correspond fittingly with the measured values. This indicates the correct functionality of the pressure adjustment spool model and pressure relief valve model. Pressure drop between the pump and cylinder chambers is on correct level. Some fluctuation, visible in transition states, namely at 17.5 s, is due to the properties of the electric motor and the controller. In the simulation model, the motor speed is assumed constant, which results in different pressure curves. However, after the transition phase, the pressures are settling on the correct level. The chamber pressures correlate with the cylinder movement appropriately. Despite a minor difference in the trajectories on the position curve, the simulated average speed of the actuator corresponds to the measured speed. The difference is likely a result of inferior errors in manual dimension and weight measurements done on the excavator. It is also understandable, that since the joint friction is lumped into the cylinder friction, the behavior of friction may not be completely modeled.

The bucket and boom actuations are compared in a similar manner. The bucket cylinder was first fully retracted, then extended, and finally returned back to the fully retracted position. Respective cylinder positions and pressures are shown in Figure 21. The simulated system pressure matches the measured values, the chamber pressures are on adequate level, and the cylinder position curves are nearly identical.

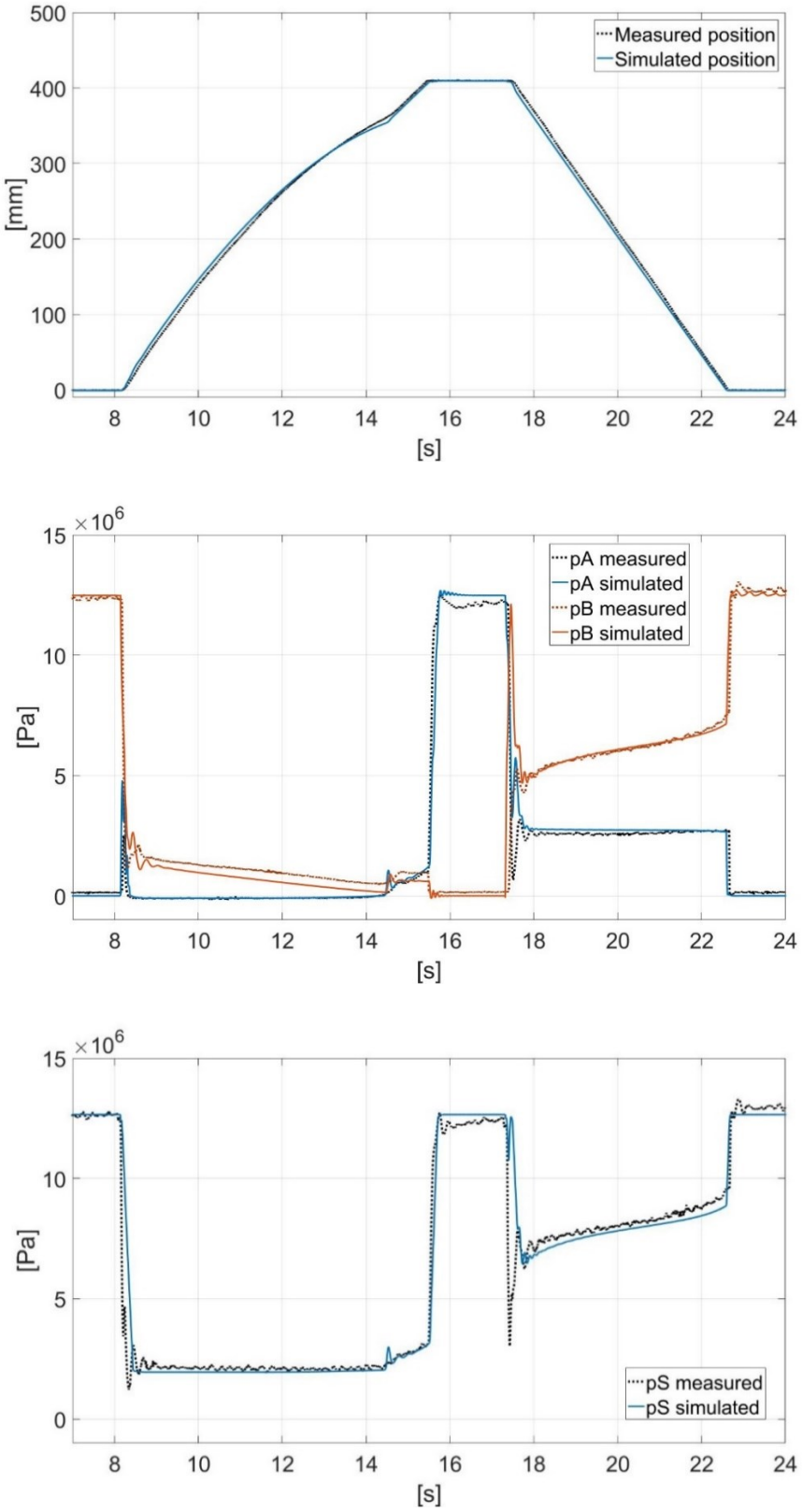

Figure 20: top: Measured and simulated arm position; middle: Measured and simulated arm cylinder chamber pressures; bottom: Measured and simulated system pressures during arm movement

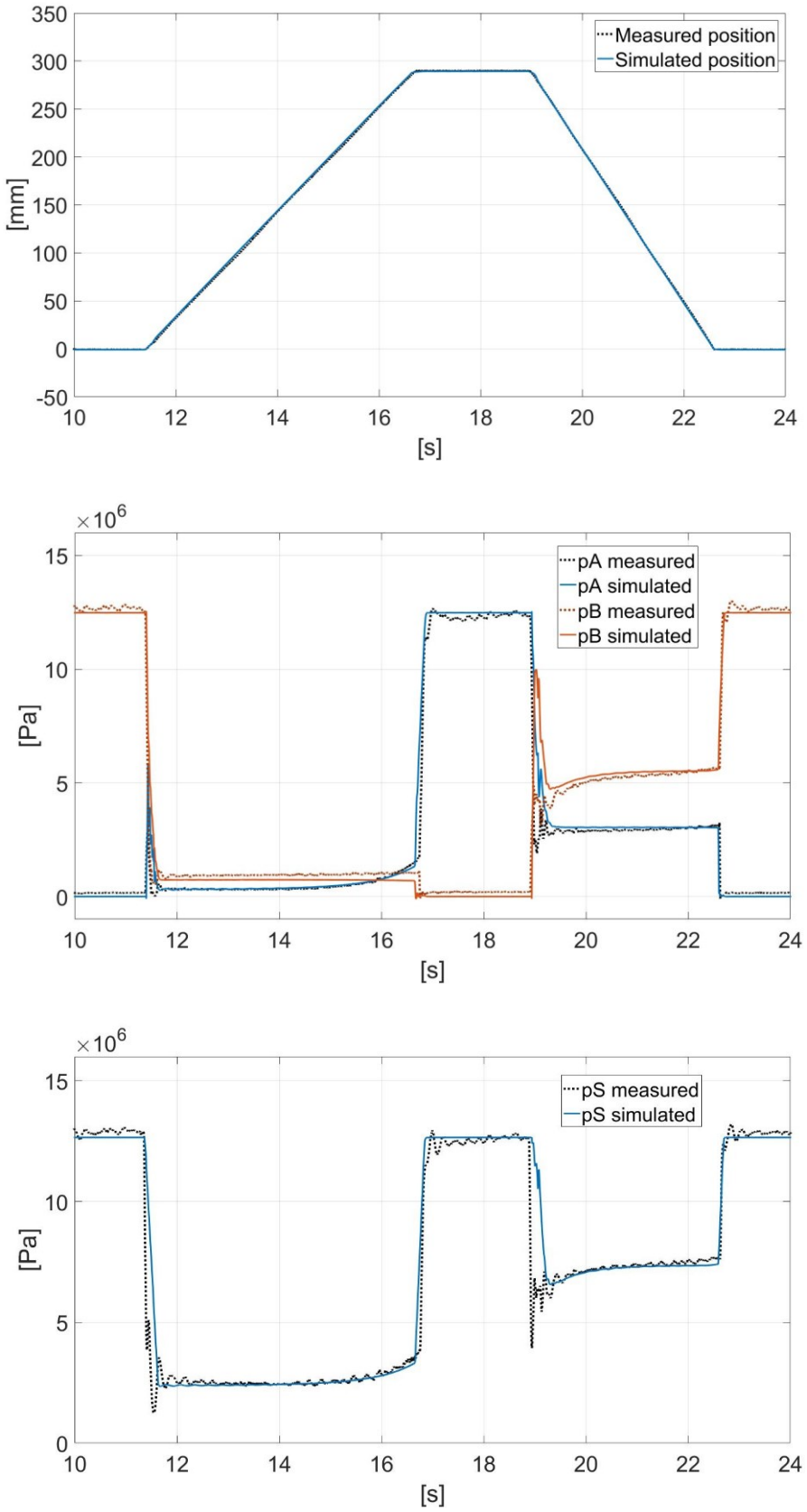

Figure 21: top: Measured and simulated bucket position; middle: Measured and simulated bucket cylinder chamber pressures; bottom: Measured and simulated system pressures during bucket movement

For the boom, it is not possible to use the full range of the cylinder length, since the bucket tooth would hit the laboratory floor in the lowest position, and the pressure transducers touch the excavator body in the highest position. Therefore, the boom is operated with the position feedback controller. The starting length of the cylinder is approximately 190 mm. It is first retracted to 30 mm and then extended back to 190 mm. Figure 22 visualizes the simulated and measured cylinder positions and chamber pressures for the boom movement. The controller affects the movement when the actuator is approaching the target position, and also when it is holding its position against the gravity. Partially opened valves complicate the fitting of the simulated and measured curves, since the valve ports do not open linearly. The pressure ports also open differently from tank ports. These opening profiles are adjusted, which is explained in section 4.1.4.

According to the verification tests, all three actuators exhibit a realistic behavior. The simulated system pressure, during the boom movement, fluctuates more than the measured pressure. This is due to minor difference between the dynamics of simulated and actual pressure adjustment valve. Most importantly, pressures settle in correct levels and the simulation converts the valve opening signals into precise actuator positions.

The simulation model is now verified with simple single-actuator maneuvers. The verification process still leaves room for improvements, and the next step would be the comparison between the simulated and measured multi-actuator movements, and applying an external load on the mechanism.

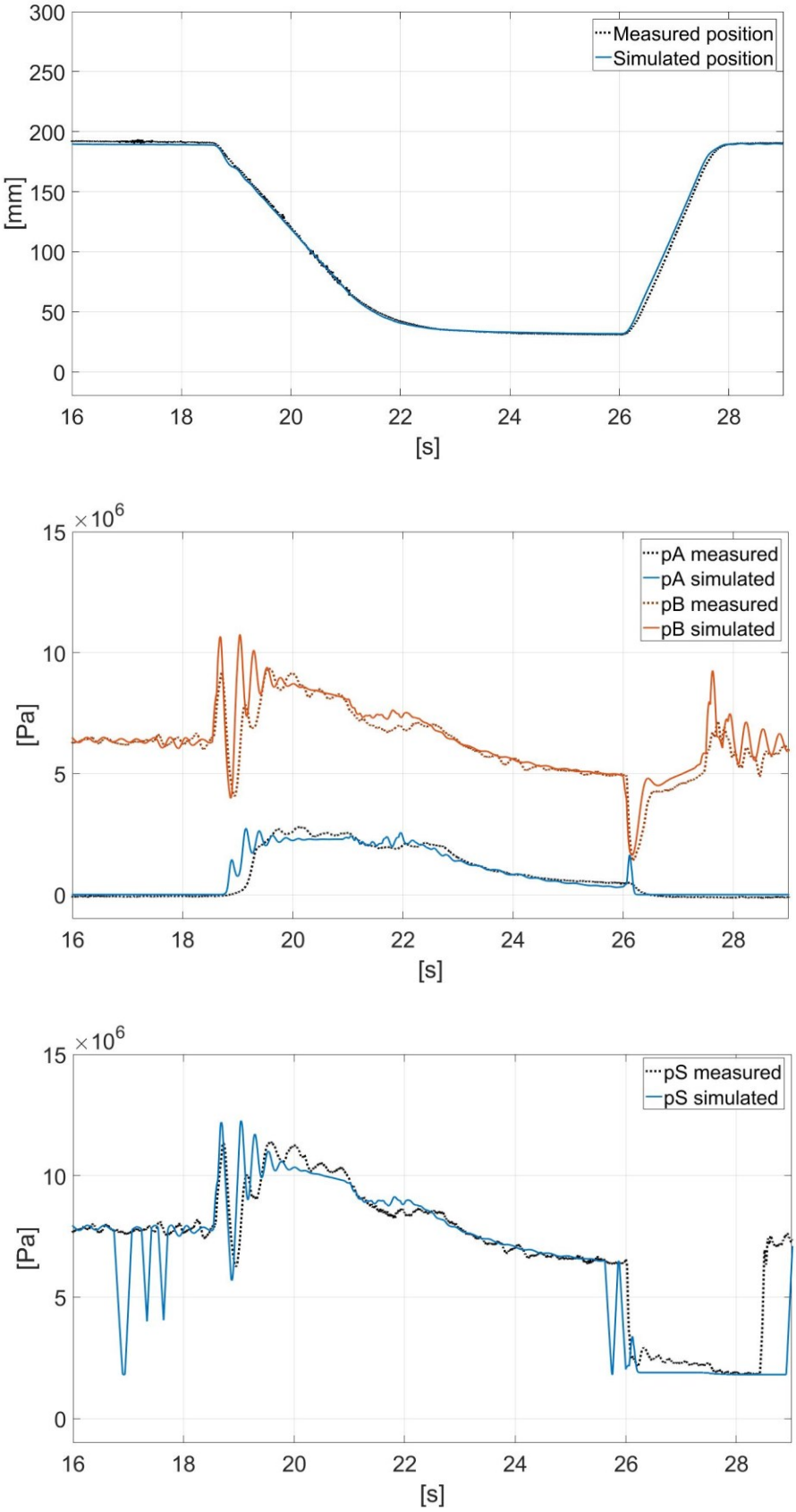

Figure 22: top: Measured and simulated boom cylinder positions; middle: Measured and simulated pressures in cylinder chambers; bottom: Measured and simulated system pressures

4.3 DDH model

The functionality of the DDH system is explained in section 2.2.1, and the simulation model is completely documented in (Järf 2016). Reader, interested in the simulation model or functionality of the DDH system, is advised to explore the Järfs thesis, since the model is not modified for this work. The hydraulic diagram of the modeled system with three DDH actuators is given in Figure 23.

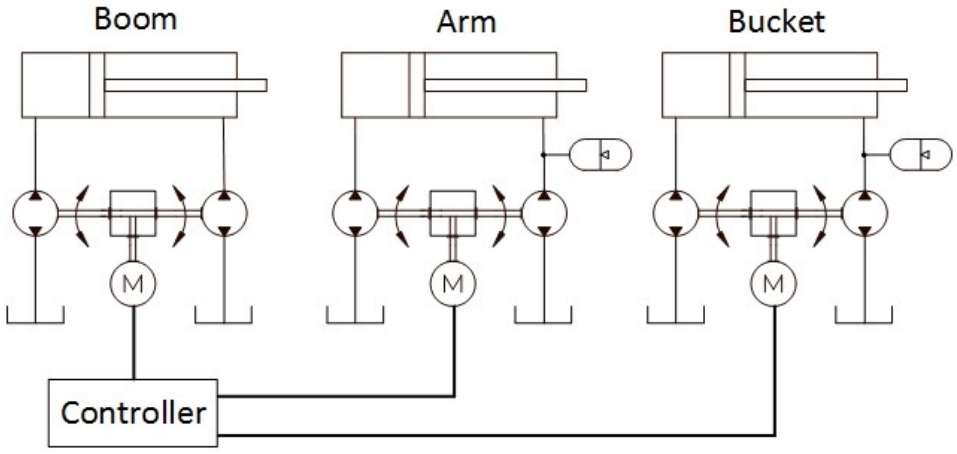

Figure 23: Simplified hydraulic schematic of the DDH system of the excavator

Järfs DDH system is dimensioned to operate a 60/30 hydraulic cylinder, which is the same size as the boom cylinder of the target excavator. The setup is realized with two pumps, which are 14.4 and 22.8 ccm/rev in size. Thus, the cylinder ratio 1:1.33 is matched with a pump ratio 1:1.58. Next question is, if the pump sizes need to be adjusted in order to operate the other two cylinders, which have a different area ratio. Arm and bucket cylinders of the excavator are of size 50/30. This results in cylinder ratio 1:1.56, which is adequately close to the pump ratio. Therefore, three identical DDH units can operate all the cylinders of the machine. The accumulator in the boom DDH actuator is disabled, since it prevents the system from carrying the gravitational force. The mass of the DDH actuators is ignored in this study, since the weight of the components and their locations are yet to be evaluated.

To model the excavator with DDH actuators, the verified conventional model is taken as the building platform, and utilized as much as possible. Thanks to the verification data, it can be assumed that the multibody model is representative for the actual machine. The cylinder models of the conventional system are utilized for the same reason. On the contrary, rest of the conventional hydraulic system is removed from the model, and replaced with three DDH models introduced in (Järf 2016). The realization of the Simulink model is shown in Figure 24. The parameters required by the model are included in Appendix C.

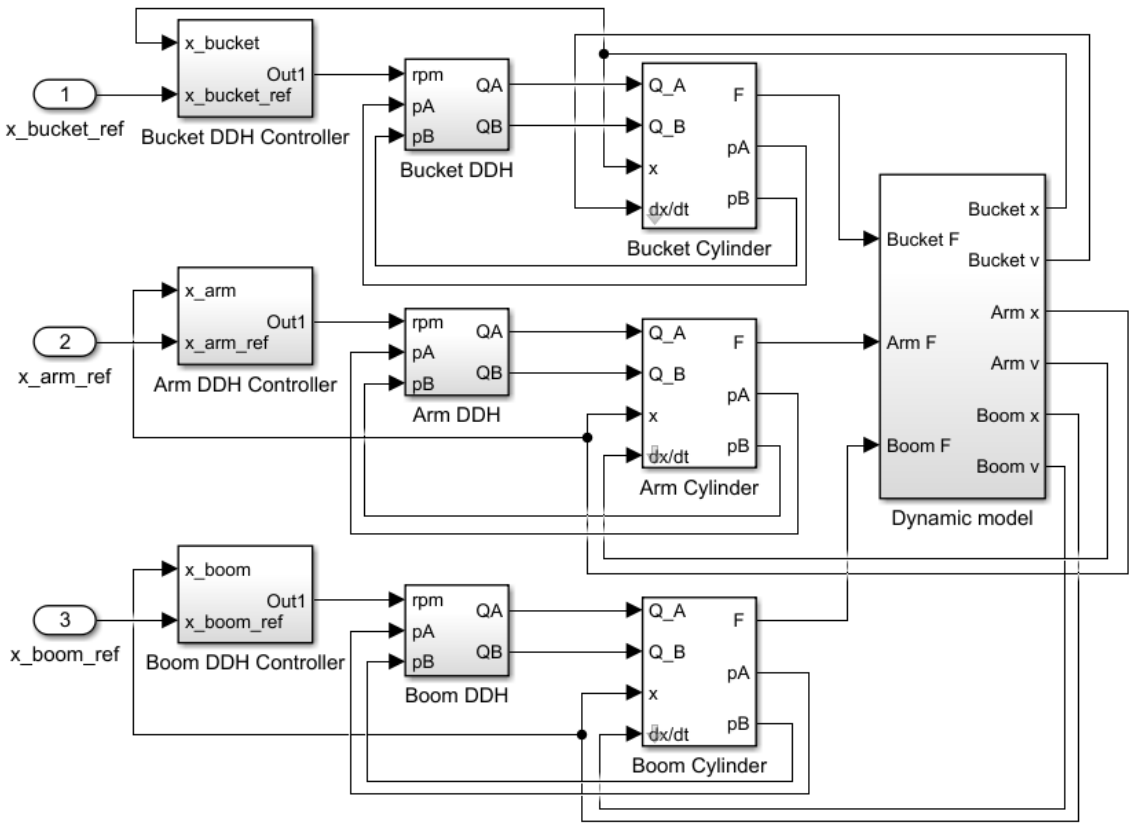

Figure 24: Simulation model with DDH actuators

5. EFFICIENCY ANALYSIS

In this chapter, the verified simulation model is utilized to study the total energy consumption and power distribution of the micro excavator. In addition to the conventional, valve controlled system, a displacement-controlled decentralized system is studied, and the results are compared and discussed. The nomenclature of the power and energy studies is explained in section 2.1. In short, the *power* refers to hydraulic power, which is the product of pressure and volumetric flow. Exceptions are pump input power, and actuator output power, both of which are mechanical power. The power distribution along the duty cycle is illustrated in graphs, to exhibit the fluctuation of the power consumption. However, an unambiguous and single-valued presentation is desired for later discussion and comparison of results. Therefore, the total energy consumption is calculated and put into tables.

Two different duty cycles, named *digging and loading cycle* and *leveling cycle*, are employed to analyze the power consumption of the excavator. The cycles are based on the standard (JCMAS 2007), and they are explained in more detail in section 2.3.1. Some limits are scaled down, due to the physical limitations of the micro excavator. In the standard, the excavators are classified based on the bucket volume. The bucket volume in the smallest class, 0.25 m^3, is still more than ten times greater than the bucket volume of the micro excavator. This affects also the reachability, so the limits, such as digging depth and loading height, were adjusted to be more suitable. In this study, the loading height is 1.2 m and digging depth 0.75 m. Since the swing motion is not included in the scope of this work, only boom, arm and bucket movements are performed. In the leveling cycle, the processing length is 1.7 m. The reference cylinder lengths for each actuator are illustrated in Figure 25.

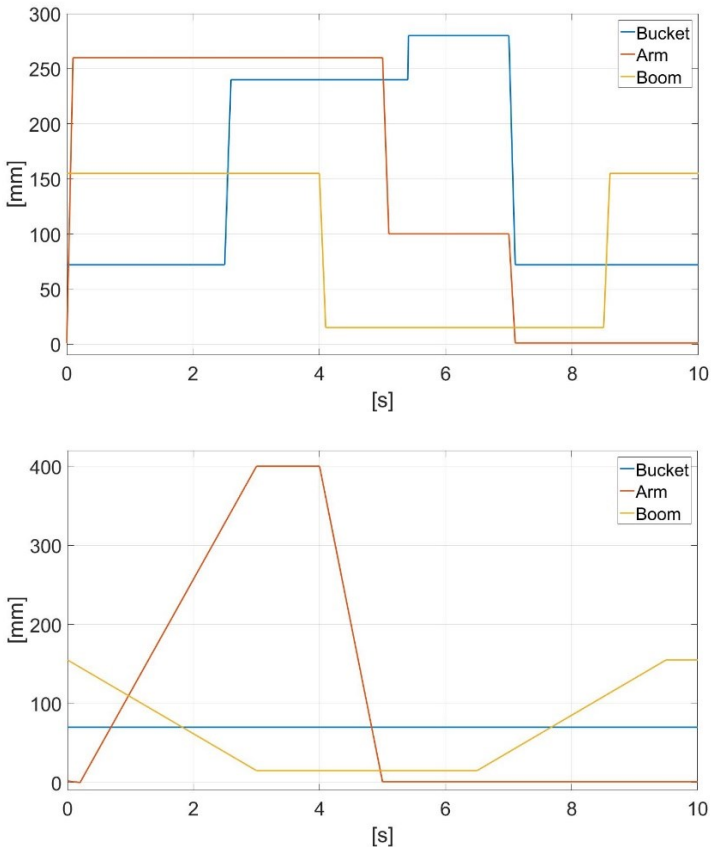

Figure 25: Reference cylinder positions for digging and loading cycle (top) and leveling cycle (bottom)

Keeping in mind the requirement for full speed, the reference position changes rapidly. This is to be sure that the actuators move as fast as possible, although intended deceleration happens near the target position, due to the nature of the controller. As the actuators in the conventional model share the constant volumetric flow, the movement speed during simultaneous movements is slower than in single-actuator movement.

5.1 Conventional system

First, the digging and loading cycle is performed. Figure 26 illustrates the power division in seven categories: pump input and output power, pressure adjustment valve (PAV), pressure relief valve (PRV), directional valve, cylinder input and power output.

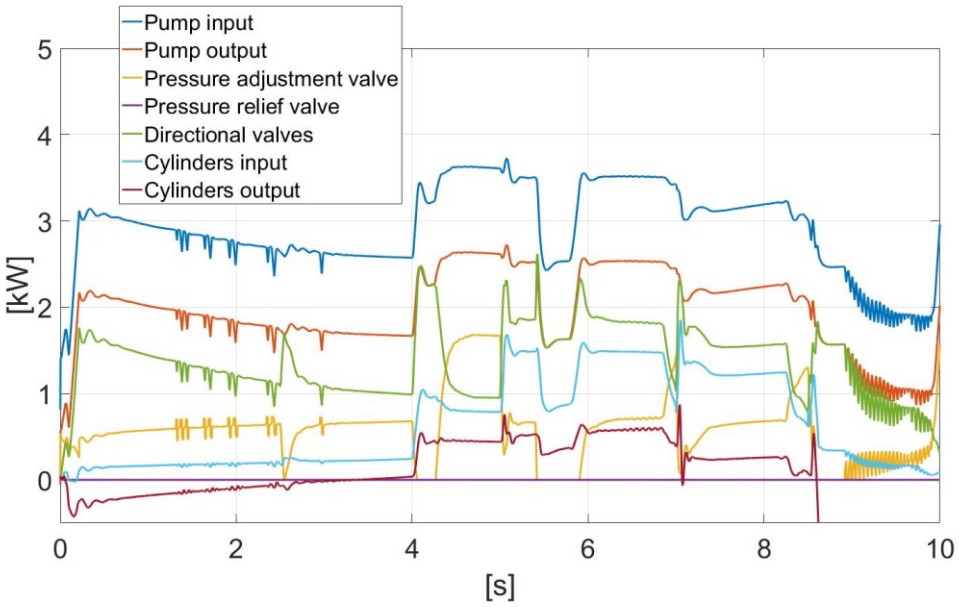

Figure 26: Power distribution in conventional system during digging and loading cycle

Pump input power, which is the same as the electric motor output, is the mechanical power employed to produce the pressure-dependent torque at the wanted rotational speed. The power model is acquired directly from a data sheet, provided by the manufacturer (Parker 2017). The pump output power is the hydraulic power leaving the pump, calculated according to equation 2. This output power is utilized in the directional valves, but a large share of it is lost, mostly in pressure adjustment valve, and throttling in directional valves. The power loss of the pump is the difference between input and output power.

The input power of the pressure adjustment valve is the product of pressure at the valve and the flow through the valve. The entire flow returns to tank, so the input power of the PAV is also the power loss of the valve. The same applies also for the pressure relief valve, although it is not opened during the test cycles.

Input power of the directional valve group is the product of flow entering the valve and the pressure at the pressure port (P) of the valve. Output power is a combination of outputs of A and B ports, and the power loss is the differential between input and output power.

The hydraulic cylinders transform the hydraulic energy into the actuator work. Losses are caused mainly by the backpressure and mechanical friction. The input power is solely hydraulic power. Output power is a combination of mechanical output power and the hydraulic power leaving the cylinder. The volumetric flow out of the cylinder is somewhat problematic. In an ideal system, the leaving flow would jump into the tank in zero pressure. In realistic system, however, the return flow runs through the hoses and valves, which results in a significant pressure rise at the cylinder chamber, the backpressure. It causes a force opposite to working direction, and reduces the net force

derived from the actuator. Therefore, using plain net force to calculate the output power gives too disadvantageous picture of the cylinder efficiency. Instead, the leaving flow is count into the output power of the cylinder. The power loss is the differential between input and output power. Power losses are collected in the Table 3.

Table 3: Energy losses in conventional system during digging and loading cycle

	Total input	**Pump losses**	**Pressure adjustment valve**	**Directional valves**	**Hoses**	**Actuator losses**	**Actuator work**
Energy [J]	28 936	9 320	5 852	10 943	2 599	691	10
Share of total loss [%]	100.00	32.21	20.22	37.82	8.98	2.39	0.03

If count together, the sum of all losses matches the total input energy, which indicates a correct functionality of the simulation model. The actuator work is close to zero, because the machine returns to the starting posture in the end of the cycle, where the potential energy is also the same as in the beginning.

As for the digging and loading cycle previously, Figure 27 shows the power distribution by components during leveling cycle.

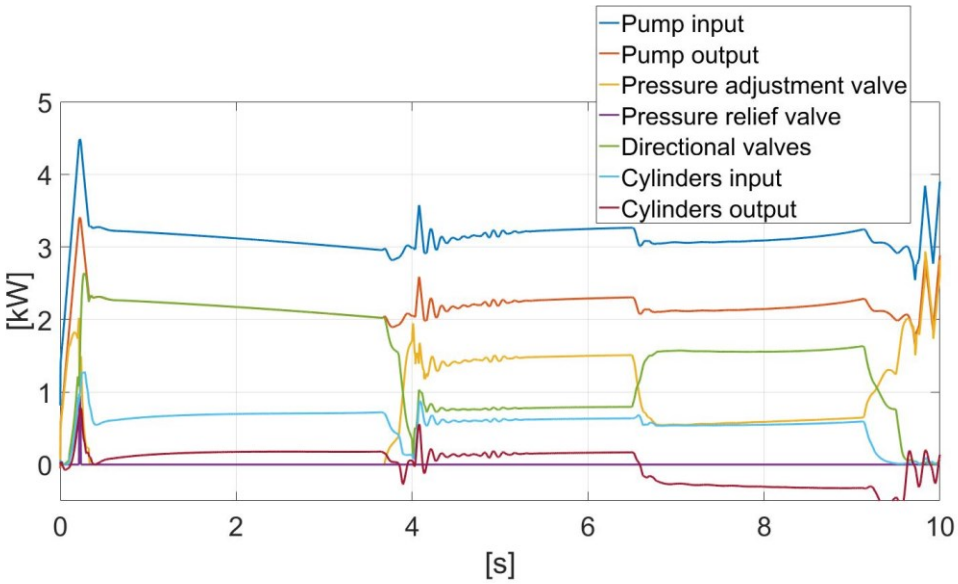

Figure 27: Power distribution in conventional system during leveling cycle

A similar energy loss calculation is performed, results of which are collected in the Table 4.

Table 4: Energy losses in conventional system during leveling cycle

	Total input	Pump losses	Pressure adjustment valve	Directional valves	Hoses	Actuator losses	Actuator work
Energy [J]	31 251	9 483	7 307	12 089	2 201	646	-7
Share of total loss [%]	100.00	30.34	23.38	38.68	7.04	2.07	-0.02

In this cycle, the actuator work is on the negative side. Compared to the total input energy, the value is still negligible, denoting that the potential energy at the end position is the same as in the beginning of the cycle.

The results for the conventional system are consistent between the two duty cycles. The directional valve is the main energy consumer with 38-39% of total energy. Together with the PAV losses, the total energy lost in the valve group is 58-62%. Pump losses, which include the mechanical and volumetric losses, account for 30-32%. The rest of the input energy is lost in frictions of hoses (7-9%) and cylinders (2%).

5.2 DDH system

For the conventional system, the actuator speed during simultaneous movements is slower than in single-actuator movement. To compensate this, the reference position profile for DDH system is modified to make the DDH system produce the exact same movement (and output work) as the conventional one. First, the digging and loading cycle is executed. The reference and simulated positions of both conventional and DDH system are plotted in Figure 28.

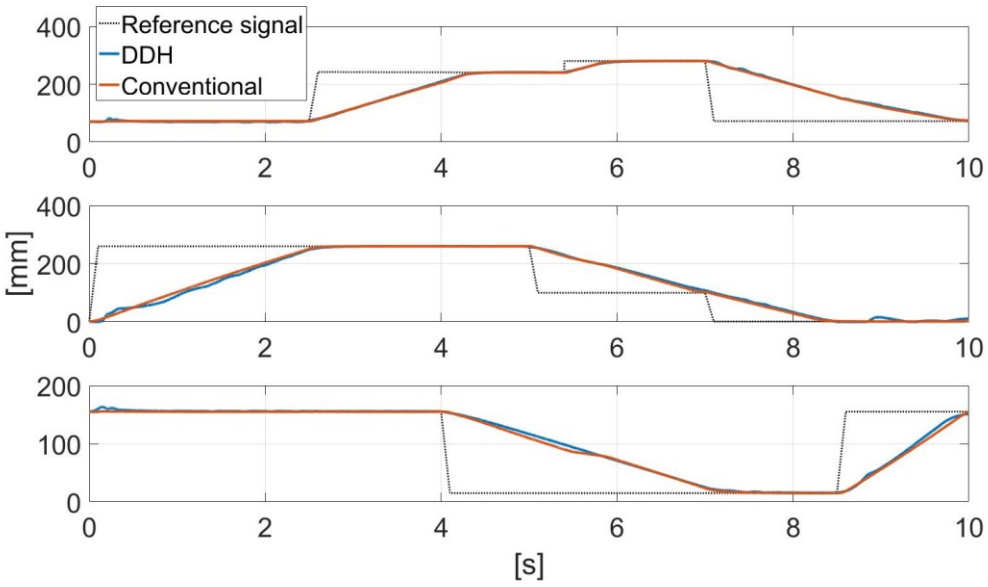

Figure 28: Reference cycle and simulated trajectories of conventional and DDH systems in digging and loading cycle. From top to bottom: bucket, arm, boom.

The figure points out the practically identical trajectories of all three actuators for both conventional and DDH systems. As the same mechanical model is utilized, also the output actuator work is identical. The power distribution within the DDH system is shown in Figure 29 in the same manner as for the conventional system in previous section. The curve includes the total power of all three actuators (boom, arm and bucket).

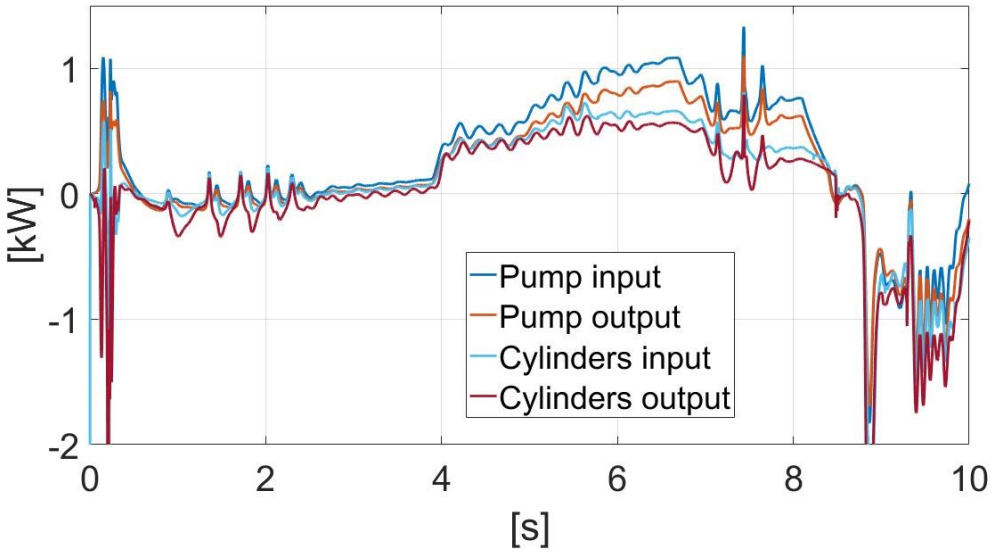

Figure 29: Power distribution in DDH system during digging and loading cycle

The higher performance of the DDH system enables it to follow the reference signal closer. Therefore, it oscillates around the target position, which is visible also in the power consumption figure. The total energy consumption by components is collected in Table 5

Table 5: Energy losses in DDH system during digging and loading cycle

	Total input	Pump losses	Accumulators	Hoses	Actuator losses	Actuator work
Energy [J]	2 717	844	593	125	885	17
Share of total loss [%]	100,00	31,06	21,83	4,60	32,57	0,63

If count together, the sum of all losses is 91%. The possible factors behind the missing 9% are discussed in the next section. After the digging and loading cycle, the leveling cycle is investigated with DDH system. The reference signal, and the simulated trajectories of conventional and DDH system are plotted in Figure 30 to point out the matching actuator movement.

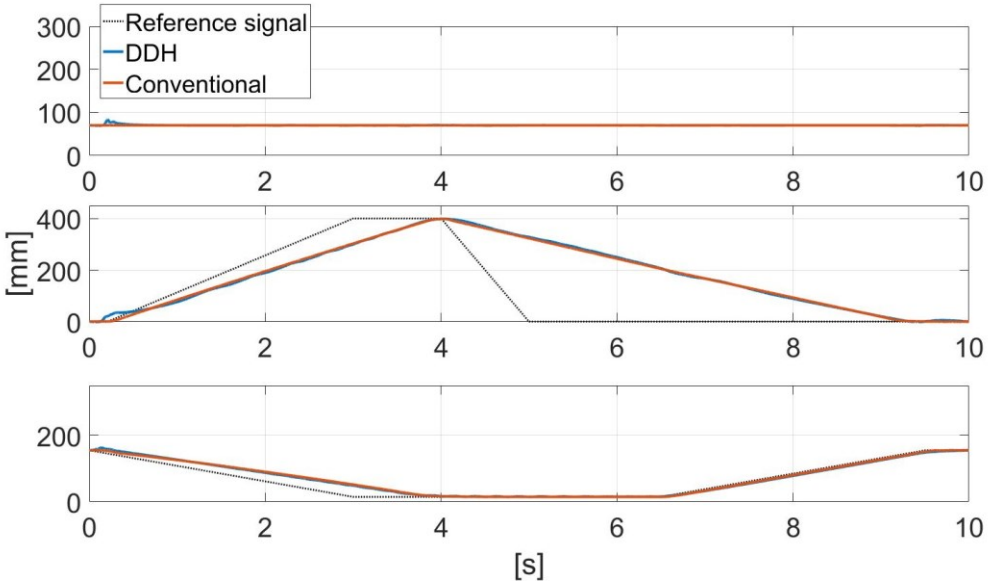

Figure 30: Reference cycle and simulated trajectories of conventional and DDH systems in leveling cycle. From top to bottom: bucket, arm, boom.

The power distribution in the DDH system is shown in Figure 31. The figure includes the total power of all three actuators.

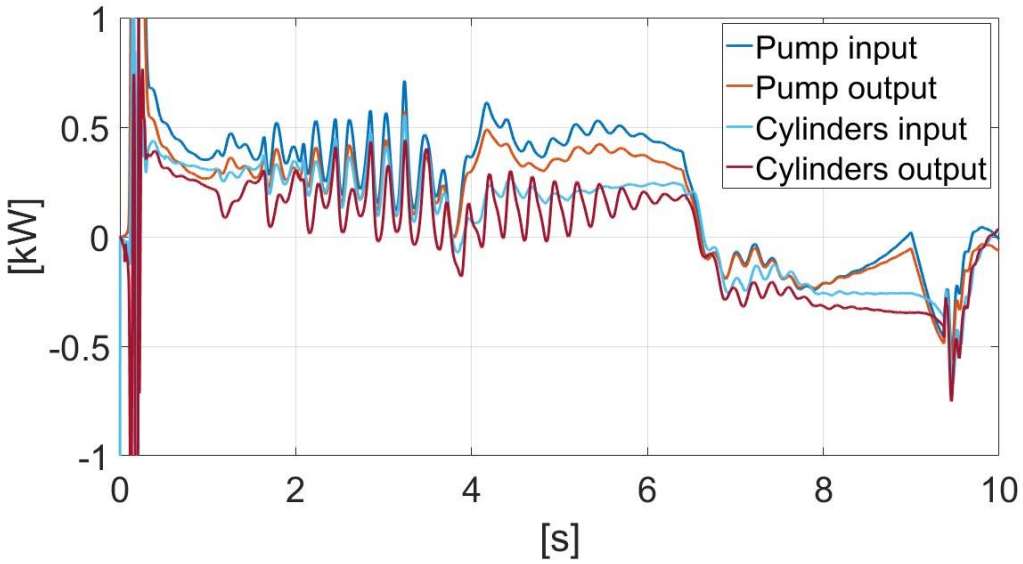

Figure 31: Power distribution in DDH system during leveling cycle

The oscillation, resulting from proximity of the target position, is visible also in this figure, especially at 2-4 seconds. The total energy consumption by components is collected in Table 6.

Table 6: Energy losses in DDH system during leveling cycle

	Total input	Pump losses	Accumulator	Hoses	Actuator losses	Actuator work
Energy [J]	2 347	687	544	91	794	3
Share of total loss [%]	100,00	29,27	23,18	3,88	33,83	0,13

5.3 System comparison

Study results, the relative energy losses, are collected in Table 7. For simplicity, average values between two duty cycles are used.

Table 7: Relative energy distribution

	Conventional	DDH
Pump	31.3%	30.2%
Accumulator	0.0%	22.5%
Directional valves	38.3%	0.0%
PAV	21.8%	0.0%
Hoses	8.0%	4.2%
Actuator losses	2.2%	33.2%

The pumps contribute for approximately 30% of the total energy loss in both systems. This is expected result for the conventional system, but since the DDH system consists of 6 pumps in total, two pumps for each actuator, a larger share of total losses was expected in that system. The directional valve is undoubtedly the main cause of energy loss in the conventional system, even more so if also the pressure adjustment valve is count as a part of directional valve. In that case, the valve block is responsible for over 60% of the total energy loss. The accumulators of the DDH system consume 22.5% of the total energy. In the conventional system, 8% of the energy is lost in hoses and other flow paths. In the DDH system, the amount of hoses is significantly lower, which explains the smaller share of the hose losses. Actuators consume a larger proportion of the total energy in the DDH system, but the absolute energy is of the same order of magnitude.

As surely seen in previous sections, the DDH system consumes only a fraction of the energy consumed by the conventional system. The average input energy was decreased by 91.6%, from 30 kJ to 2.5 kJ. Explaining the difference with the absence of the directional valves is tempting, but is does require some closer examination. The total input powers of the two systems are plotted together in Figure 32.

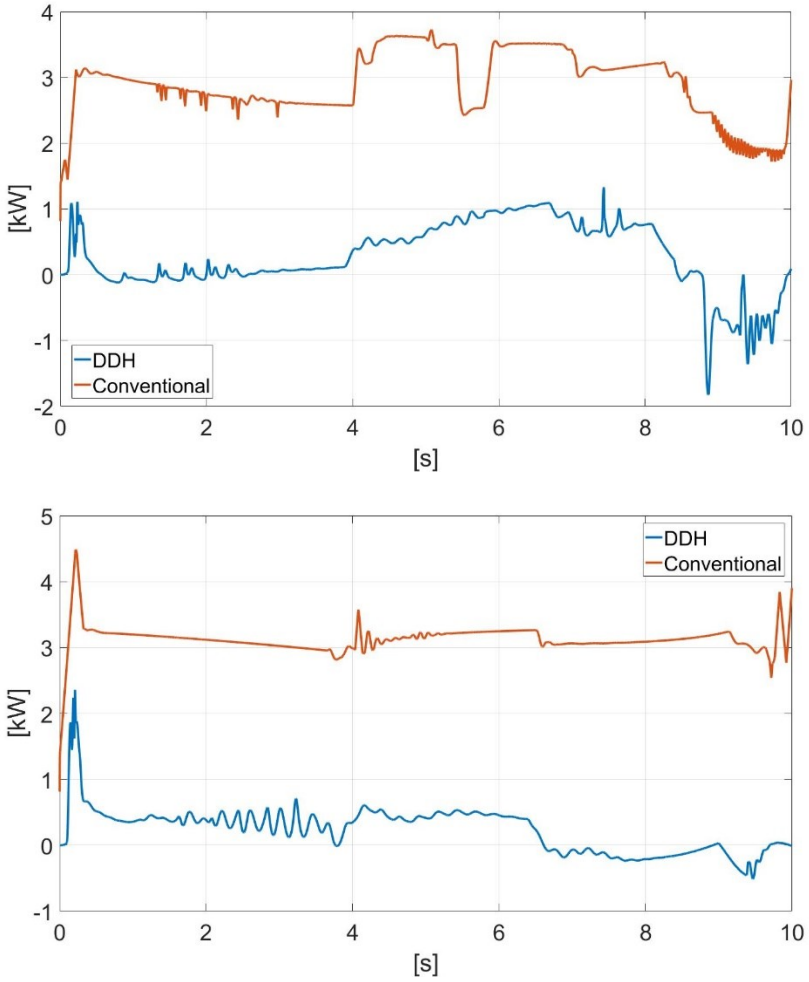

Figure 32: Power consumption of conventional and DDH model in digging and loading cycle (top) and leveling cycle (bottom)

The dramatic difference between the power consumptions of the two systems raises a question for the reason behind the divergence. Next, the hydraulic input powers of the arm cylinders in both systems are plotted for comparison in Figure 33. Since the cylinder models are identical, and they perform virtually the same movement, their power consumption would be expected to be the same, but the power loss of the valve controlled system is visibly higher at 0-2.5 seconds and 5-8.5 seconds, which are the moments of actuator work.

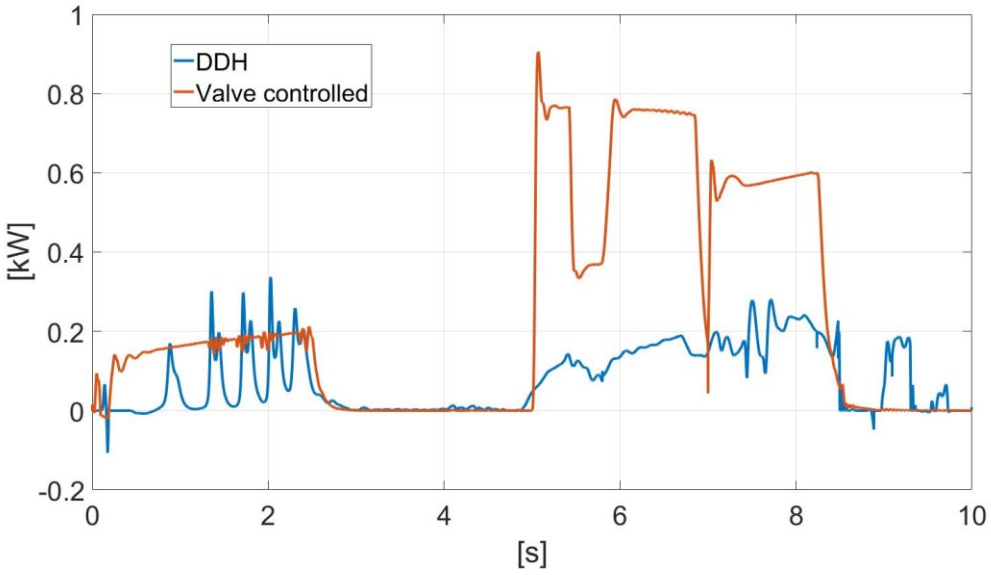

Figure 33: Arm input power in DDH and valve controlled system

The primary cause for the difference is the higher backpressure in the non-working chamber in the valve-controlled system. To demonstrate this, the arm chamber pressures for both systems are plotted in Figure 34.

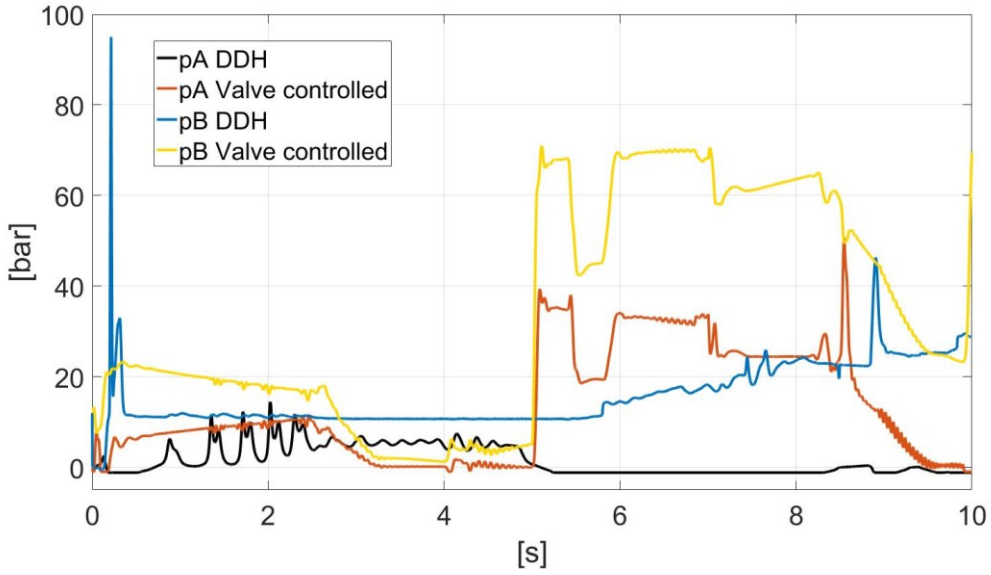

Figure 34: Simulated chamber pressures in arm cylinder

The backpressure is the result of flow losses, in the hoses and valves, between the cylinder and the tank. In an ideal situation, the leaving oil volume would just jump into the tank in an atmospheric pressure. In the DDH system, the secondary pump is actually working to remove the excess oil from the cylinder, unless the oil pressure is high enough to make the work into the system, which is, in practice, energy recovering. In the conventional

system, the oil flow to the tank is lost energy, and the more it is throttled, the more energy is lost.

5.4 Discussion

The results strongly underline the outstanding efficiency of the DDH system, and, on the other hand, indicate a great room for improvement concerning the conventional system. The test case, however, is not completely fair. First, the poor efficiency of a LS system during multiple actuator movement is commonly known. The system pressure is adjusted according to the highest load, and the flow into the other actuators is throttled. In addition, the fixed-volume pump of the micro excavator does not adjust the output flow, as in LS systems, but produces a constant flow. A remarkable portion of the flow is wasted through the pressure adjustment valve, to keep the system pressure level low, according to the low loading condition. According to the simulation, more than 20% of the total power is lost in PAV only. This result calls for more research, and an experimental setup is being prepared to test the excavator in realistic contact with earth. The variable ground contact force will be recorded, and added in to the simulation model, as presented in (Williamson et al.).

Movement speed of the excavator is dependent on the rotational speed of the electric motor. Increasing the speed would, in this test case, result in more volume lost in PAV. With a more realistic loading condition, in which the PAV would stay unopened most of the time, the additional volumetric flow could be utilized in increased movement speed. This would reduce the cycle time and possibly improve the overall efficiency. The electric motor speed is assumed constant in the simulation model. Additional speed and torque sensor will be fitted for more accurate information on the motor dynamics. A current sensor, which will produce data on the total input energy, will also be prepared for upcoming research.

The accumulators of the DDH system consume 22.5% of the total energy, when the cycle was driven one time. If more cycles were to be driven, the effect of the accumulators could be diminished, if they are filled only during the first cycle. Therefore, the effect of the accumulators calls for more detailed investigation.

The actuator losses, which are caused by the frictions in cylinders and the joints of the front hoe, account for only 2% of the total losses in the conventional system. This has, so far, given little or no incentive for further research. In the DDH system, on the contrary, the share of frictional losses is remarkably larger (33%). Although the study may give an overly positive picture of the efficiency of DDH units, it seems evident that there will be rising demand for low-friction mechanical solutions. The friction model could be improved by adding a pressure-dependent component and an angular speed-dependent component, since the current model does not take pressure in to account, and the friction is now a function of cylinder speed only.

The weight redistribution related to the application of DDH units is not took into consideration within this analysis. The weight of the central pumps and the electric motor would be removed, but the weight of all DDH units would be added. Unlike the centralized mass of the conventional power pack, which, in fact, stabilizes the machine, the additional weight of the DDH units is decentralized, and added into the moving load of the front hoe. The magnitude of this disadvantage depends on the DDH component selection, and can be minimized with optimal placement of the units, but needs anyway to be taken into account when comparing the real benefits of the DDH technology.

6. CONCLUSIONS

A Simulation model of the electro-hydraulic excavator is produced. The model consists of the hydraulic and mechanical systems related to actuation of front hoe, i.e. boom, arm, and bucket. Model parameterization is based on measurement data, when available, and the information found in the literature.

The excavator is fitted with pressure and position sensors, from which the information is collected with a data acquisition system. In addition, a CAN-interface is established, in order to communicate with aftermarket directional valves the excavator is fitted with. Comprehensive communication system enables the verification of the simulation model, which gives weight on the obtained results.

The verified simulation model is utilized to study the total energy consumption and power distribution of the micro excavator. In addition to the conventional, valve controlled system, a decentralized, displacement-controlled system, realized with direct-driven hydraulic units, or DDHs, is studied, and the results are compared and discussed. Two different duty cycles, named *digging and loading cycle* and *leveling cycle*, based on the JCMAS standard, are used to analyze the power consumption of the excavator.

The results indicate a formidable room for improvement concerning the conventional system, since a power loss of as much as 60% is generated in the directional valve group. The DDH system seems to be a promising solution to improve the efficiency of the excavator. A total power consumption of the DDH system is less than 10% of the consumption of the conventional system, during two different free-space duty cycles. Subsequently, results of this study will motivate for further research and for manufacturing a working prototype.

Suggested next phase of the research would be the application of external load into the duty cycle. The poor efficiency of a LS-system during unloaded multi-actuator movements is a well-known fact, and operating in this area will give a too negative picture of the efficiency of the conventional system. A ‘sandbox’ test area for reproducing the ground contact is being planned, and the load sensors will be attached in all cylinder pins for accurate load measurement.

The simulation model could be improved with a more accurate model of the electric motor. An additional speed-torque sensor will be installed to acquire information on the motor dynamics, and a current sensor, which will produce data on the total input energy, will be prepared for upcoming research. The actuator losses, which are caused by the frictions in cylinders and the joints of the front hoe, account for 33% of the total losses in the DDH system. This adds more focus towards the friction study, and the simulation

model could be improved, by adding pressure-dependent and angular speed-dependent variables. In the DDH system, also the effect of the accumulators need more investigation, as they consume 22.5% of the total energy, according to the simulation.

REFERENCES

Avci, A., Karagoz, I. A Novel Explicit Equation for Friction Factor in Smooth and Rough Pipes. Journal of Fluids Engineering, Vol. 131. 2009, ASME

Bak, M.K., Hansen, M.R. Modeling, Performance Testing and Parameter Identification of Pressure Compensated Proportional Directional Control Valves. University of Agder, Norway.

Canudas de Wit, C., Olsson, H., Åström, K. J., Lischinsky, P. A New Model for Control of Systems with Friction. IEEE Transactions on Automatic Control, vol. 40, no. 3, March 1995.

Danfoss. Proportional Valve Group PVG 32, Technical Information. 520L0344. Danfoss. March 2016.

Ellman, A., Piché, R. A Modified Orifice Flow Formula for Numerical Simulation of Fluid Power Systems. FPST-Vol. 3, Fluid Power Systems and Tevhnology: Collected Papers. ASME 1996.

Hassi, T., Korva, A., Markkula, S., Partanen, T., Sourander, T., Kiviluoma, P., Korhonen, A. & Kuosmanen, P. Improving Energy Efficiency of an Electric Mini Excavator. 11th International DAAAM Baltic Conference, Industrial Engineering, 20-22th April 2016, Tallinn, Estonia

Henriksen, D. Design and Construction of a Facility for Testing Friction in Hydraulic Cylinders. Aalborg University, 2009.

Hippalgaonkar, R., Ivantysynova, M. A Series-Parallel Hydraulic Hybrid Mini-Excavator with Displacement Controlled Actuators. The 13th Scandinavian International Conference on Fluid Power, SICFP2013, June 3-5, 2013, Linköping, Sweden.

Hyvönen, M. Hydraulikomponenttien mallintaminen ja simulointi. Lecture notes for course IHA-2601: Modelling of Fluid Power Components. 2015.

Irving, M., Tammisto, J., Hodgson, E.R., Hernández, T. Irradiation and testing of off-the-shelf seal materials for water hydraulic applications in ITER remote handling equipment. Fusion Engineering and Design 82 (2007) 1937-1941. Elsevier Science, B.V. 2007.

JCMAS H 020:2007. Japan Construction Mechanization Association. Earth-moving-machinery – Fuel consumption on hydraulic excavator – Test procedures.

Järf, A. Flow compensation using hydraulic accumulator in direct driven hydraulic differential cylinder application and effects on energy efficiency. Master's thesis. Aalto University, School of Engineering. Espoo, 2016.

Järf. A., Minav, T., Pietola, M. Nonsymmetrical Flow Compensation Using Hydraulic Accumulator in Direct Driven Differential Cylinder Application. Proceedings of the ASME 2016 9th FPNI Ph.D. Symposium on Fluid Power. FPNI2016, October 26-28, 2016, Florianópolis, SC, Brazil.

Kauranne, H., Kajaste, J., Vilenius, M. Hydraulitekniikka. 1.Painos. WSOY Oppimateriaalit Oy. 2008, Helsinki, Finland.

Ketonen, M., Linjama, M. Simulation study of a digital hydraulic independent metering valve system on an excavator. The 15th Scandinavian International Conference on Fluid Power, SICFP'17, June 7-9, 2017, Linköping, Sweden.

Kiviranta, J. Instrumentation of an Automated Excavator. Master's Thesis. Helsinki University of Technology, 2009.

Kvaser. J1939 Introduction. https://www.kvaser.com/about-can/higher-layer-protocols/j1939-introduction/. Visited on 8 September, 2017.

Lin, T., Wang, Q., Hu, B., Gong, W. Development of Hybrid Powered Hydraulic Construction Machinery. Automation in Construction 19 (2010). pp 11-19. Elsevier.

Maharjan, D., Mahat, C., Liljeström, J., Vauhkonen, N., Kiviluoma, P., Kuosmanen, P., Sainio, P. Electrification of Excavator. 9th International DAAAM Baltic Conference "Industrial engineering" 24-26th April 2014, Tallinn, Estonia.

MathWorks. Model and simulate multibody mechanical systems. https://se.mathworks.com/products/simmechanics.html. Visited on 29 August, 2017.

Olsson, H., Åström, K. J., Canudas de Wit, C., Gäfvert, M., Lischinsky, P. Friction Models and Friction Compensation. European Journal of Control (1998) 4:176-195. 1998 EUCA.

Parker Hannifin Corporation. Gear Pumps/Motors, Series PGP/PGM Fixed Displacement Pumps, Cast-Iron and Aluminium Designs. Catalogue HY30-3300/UK. 2017 Parker Hannifin Corporation.

Sevcon. Gen4 Applications Reference Manual, Document no: 177/52701. Rev.2.

Siko. Vaijerianturi SGH10. Datasheet. Available at http://www.sks.fi/www/sivut/4F4E733253B81BDFC2257B5B005F8E19/$FILE/siko-sgh10-kv1h-datalehti-2016-08-23.pdf. Visited on 29 August 2017.

Siuko, M., Pitkäaho, M., Raneda, A., Poutanen, J., Tammisto, J., Palmer, J., Vilenius, M. Water Hydraulic Actuators for ITER Maintenance Devices. Fusion Engineering and Design 69 (2003) 141-145. Elsevier Science B.V. 2003.

Vukovic, M., Leifeld, R., Murrenhoff, H. Reducing Fuel Consumption in Hydraulic Excavators – A Comprehensive Analysis. Energies 2017, 10, 687. MDPI. 2017.

Weber, J., Beck, B., Fischer, E., Ivantysyn, R., Kolks, G., Kunkis, M., Lohse, H., Lübbert, J., Michel, S., Schneider, M., Shabi, L., Sitte, A., Weber, J., Willkomm, J. Novel System Architectures by Individual Drives. 10th International Fluid Power Conference, Dresden, 2016.

Williamson, C., Zimmerman, J., Ivantysynova, M. Efficiency Study of an Excavator Hydraulic System Based on Displacement-Controlled Actuators. Purdue University, Department of Agricultural and Biological Engineering, West Lafayette, Indiana, USA.

Zimmerman, J.D., Pelosi, M., Williamson, C.A., Ivantysynova, M. Energy Consumption of an LS Excavator Hydraulic System. Proceedings of IMECE2007, 2007 ASME International Mechanical Engineering Congress & Exposition. November 11-15, 2007, Seattle, Washington, USA.

APPENDIX A: INSTRUMENTATION OF DATA ACQUISITION AND CONTROL SYSTEM

This appendix describes the measurement, control, and data acquisition system. Physical measurements on the excavator provide data for parameterization and verification of the simulation model. The excavator is fitted with pressure sensors in all cylinder ports and in the pump outlet port, and position sensors at the cylinder rods. The measurement signals are collected and recorded at a target-pc. The physical structure of the system is shown in Figure 35. Communication channels are visualized as lines, with the text pointing out the communication protocol. Boxes with solid line represent hardware and boxes with dotted line are software.

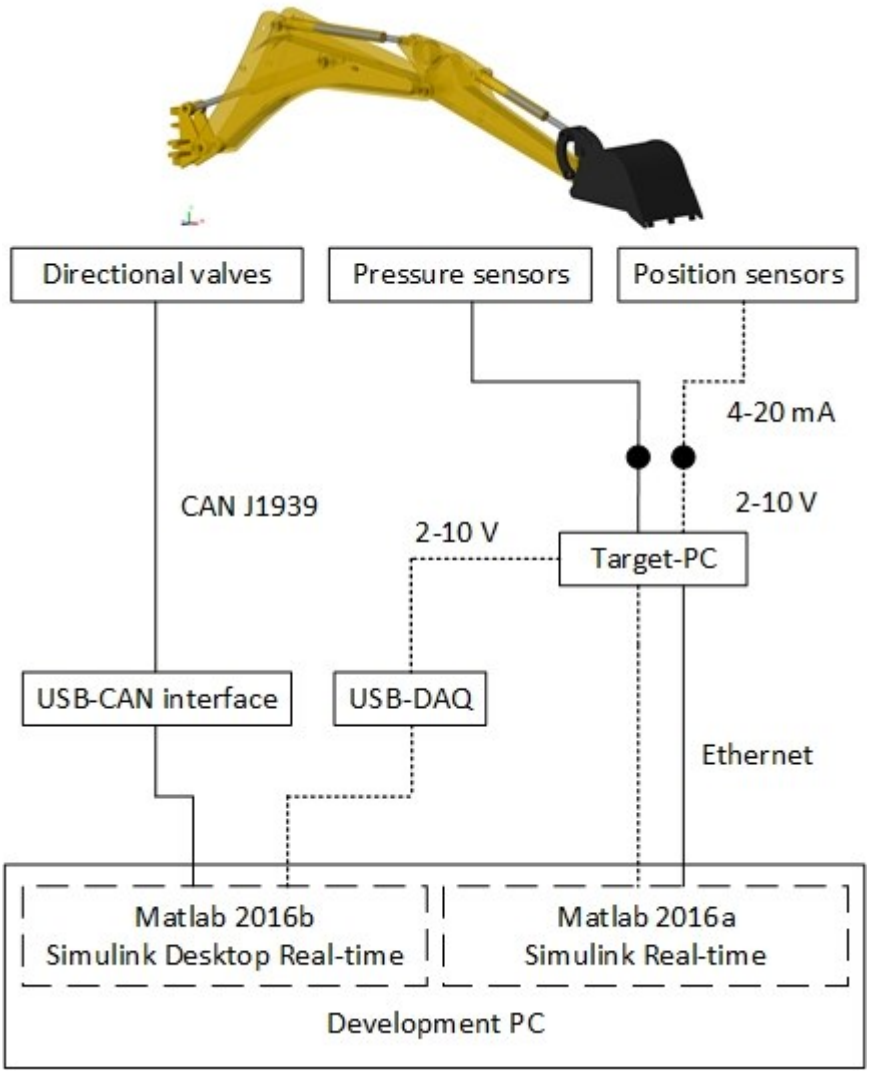

Figure 35: Measurement, control, and data acquisition system of the excavator

Simulink Real-Time -toolkit enables creating real-time applications from Simulink models. They run on a dedicated target computer, which is connected to the physical system via analog I/O ports. In this project, the real-time application is used to collect the

time-synchronized measurement data from pressure transducers and position sensors, and to communicate with the directional valves.

The Danfoss PVG 32 valves are equipped with electro-hydraulic control modules PVED-CC. Communication between valves and computer uses CAN J1939 protocol. Simulink provides blocks necessary to communicate with the bus, and, together with the real-time kernel, enables driving the model in real-time, without having to use an additional target pc. The time synchronization toolkit is called Simulink Desktop Real-time, which is, for practical reasons, run on Matlab version 2016b.

The target-pc is connected to a Windows-pc (also called *development computer*) via an Ethernet cable. The user creates the Simulink model, which includes the blocks required to collect the measurement data, builds the model, and starts the model on the target-pc via a Simulink Real-time application. This user interface is run on Matlab version 2016a.

All the measurements are done in laboratory environment, so the conditions, such as humidity and temperature, are considered constant. The excavator is used for relatively short periods of time, and it is equipped with a water cooling system. Therefore, the effect of possible temperature rise during operation is assumed negligible.

Control of CAN valves

The Danfoss PVG 32 valves are equipped with electro-hydraulic control modules PVED-CC. Communication between valves and computer happens over CAN J1939 protocol. The selected user interface is Matlab Simulink. It provides blocks necessary to communicate with the bus, and, together with the real-time kernel, makes it possible to drive the model in real-time, without having to use an additional target pc. The USB-CAN interface is Vector VN1610.

J1939 protocol in a nutshell

A J1939 message can be divided in two parts: the identification (ID) and the message part. The ID is a 29-bit long string of bits. It includes information on the message priority, purpose, sender and intended receivers. As an example, a message used commonly in this project, Auxiliary Valve Command (AVC), is explained. The structure of the ID is depicted in Table 8. The messages are typically represented in hexadecimals, although the interpretation often requires transforming them first in binary numbers and later in decimals.

Table 8: The structure of the ID number in J1939 protocol

hexadecimal	0CFE3006					
binary	0000 1100 1111 1110 0011 0000 0000 0110					
bin arranged	011	0	0	1111 1110	0011 0000	0000 0110
decimal	3	0	0	254	48	6
meaning	Priority	Reserved	Data Page	PDU Format	PDU Specific	Source Address
length	3 bits	1 bit	1 bit	8 bits	8 bits	8 bits

In the AVC message, the priority, data page, and PDU format are in their default values. Reserved bit is reserved for future use and is always zero. PDU specific determines which valve is controlled: 48-63 for valves 0-15, so number 48 stands for valve number 0. Source address is the identification number of the sending device. The actual message is constructed of the ID and 8 8-bit bytes. The whole AVC message is depicted in Table 9.

Table 9: The structure of the AVC message

hexadecimal	0CFE3006	7D	00	02	00	00	00	00	00
decimal	(see table above)	125	00	2	0	0	0	0	0
meaning	ID	PFC	Res	Valve state	Res	Res	Res	Res	Res

First byte after the ID, PFC, stands for Port Flow Command. It includes a wished flow as a percentage of maximum available flow. It has a value between 0 and 255, which leads to resolution of 0.4 %/bit. Thus, the value 125 refers to flow rate of 50%. Valve state tells the direction of the flow (if any). Values used, in practice, are 0 for blocked, 1 for extend and 2 for retract direction. Other bytes are reserved and set to zero.

The communication with CAN valves starts by creating a J1939 database. The database is used to describe the properties of the network, components, messages and signals which are used on the bus. Vector CANdb++ editor is used to create and maintain the database. When messages are defined in the database file, they can be sent or received in the communication blocks of Simulink Vehicle Network toolbox. These signals can then be monitored, byte by byte, in the receive blocks at Simulink. Similarly, messages may be composed with send blocks. For example, the AVC communicates the wished flow rate in the first byte after identifier, and the wished flow direction in third byte. Normally rest of the message remains unchanged, and only these two bytes are changed during control. Individual AVC is sent to each valve in 10 ms intervals. (Kvaser)

Position feedback controller

The position signal is utilized in a closed-loop feedback system, which controls the directional valves to reach the wanted actuator position. The controller simply calculates the difference between measured position and wanted position, and commands the valves accordingly. An additional gain coefficient is used to adjust the amplification within the controller.

Data acquisition system

Physical measurements on the excavator provide data for parameterization and verification of the simulation model. The excavator is fitted with pressure sensors in all cylinder ports and the pump outlet port. Position sensors are attached to the cylinders. In measurement terminology, sensor refers to sensing component, which normally requires an additional transducer to transfer the sensor signal into standard signal, for example a voltage signal 1-5 V or a current signal 4-20 mA. Both pressure sensors and position sensors, used in this study, output a standard signal. They are, therefore, called transmitters or transducers, but in this text, referred to as *sensors*.

Pressure sensors

Hydac HDA 7446 pressure transducers are used to measure chamber pressures of each cylinder, and to transform the signal into standard current message of 4-20 mA. The sensors are calibrated by the manufacturer, and are ready to use. They are capable to measure pressure up to 250 bar, and tolerate peak pressure up to 500 bar.

The transducers are installed immediately after the cylinder ports with t-fittings and necessary adapters. They must be provided with supply voltage between 8 and 30 V and a load resistance, sized according to the supply voltage. An electrical connection presented in Figure 36 is utilized to connect the transducers with the measurement device. Current signal is transformed into voltage differential signal by directing it through a resistor and measuring the voltage over the resistor. According to Ohm's law, a current of 4-20 mA, over a 500 Ω resistor, causes a voltage differential of 2-10 Volts. The resistor size sets the lower limit of the supply voltage to 18 V. This is exceeded with external voltage source, since the DAQ device is only capable of providing supply voltage up to 5 V.

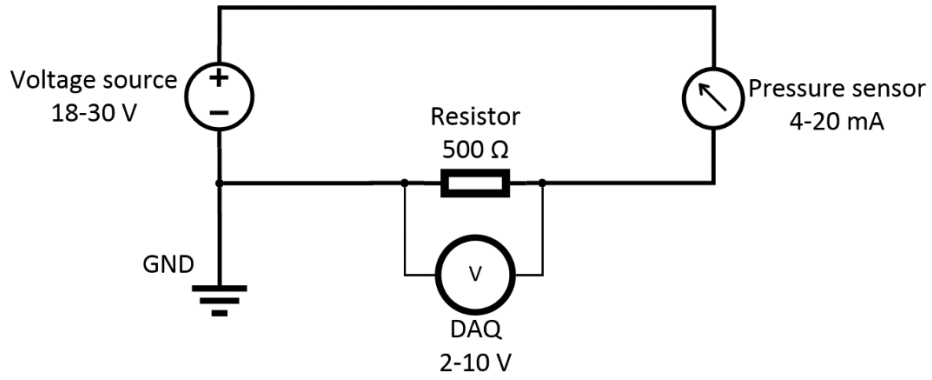

Figure 36: Electrical connection for transforming the current signal of a pressure sensor into a voltage signal

Pressure signals are collected on the data-acquisition board (National Instruments PCI-6259) of the target-pc. The device is supported hardware for Simulink Data Acquisition Toolkit, which provides easy connectability with Simulink, since the software finds and communicates with the device automatically. Sample time for pressure measurement is 1 ms. Rather noisy pressure signal is filtered using Matlab's FIR lowpass filter function to remove the rapid pressure peaks and the electrical interference of the environment (electric motor and controller, particularly).

Position sensors

The position sensors are Siko SGH10 magnetic wire sensors (Siko 2016). The sensors are intended for fitting inside a hydraulic cylinder, but since it was desired to use original cylinders without modifications, an external mounting structure was designed to fit the sensors outside of the cylinders. The SGH10 sensor measures cylinder position between 0 and 500 mm with a resolution of 0.122 mm/bit. Sensors tolerate movement speed up to 1 m/s, which is more than enough for the mini excavator measurements. The signal output is a current signal between 4 and 20 mA. Electrical connection for the position sensors, including the supply voltage and the load resistor, is identical to the connection for pressure sensors, depicted in Figure 36.

Position signals are collected on data-acquisition board (NI PCI-6259) of the target-pc. The signals are further directed to NI 6218 USB data-acquisition (DAQ) device. The device is selected due to its availability and sufficient number of analog input ports. The device is supported hardware for Simulink Data Acquisition Toolkit, which provides easy connectability with Simulink, since the software finds and communicates with the device automatically.

The physical connections of the data acquisition system are shown in Figure 37.

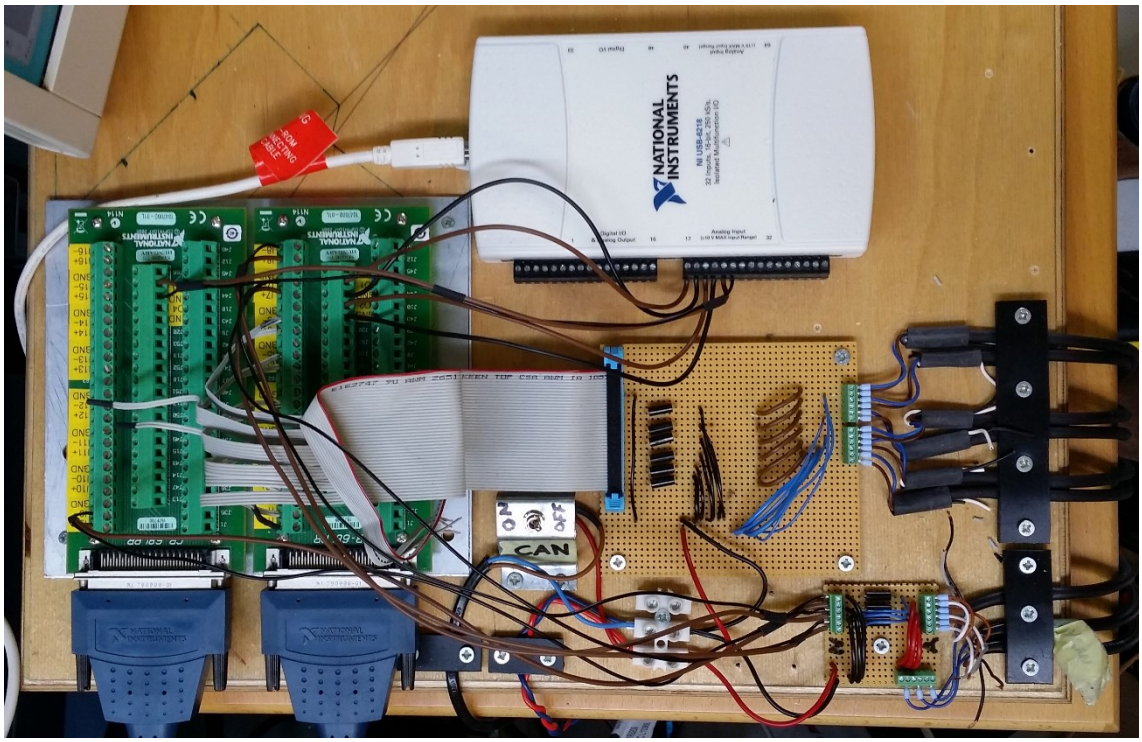

Figure 37: Measurement setup

The green terminal block, in the left part of the setup, is connecting the signals to the PCI-6259 card of the target-pc. The position sensor signals are also connected to the white USB DAQ. Brown soldering boards in the lower right part of the setup are used to connect the resistors needed to transform the current signals into voltage signals. The larger one is for the pressure sensors and the smaller one is for the position sensors. The white terminal block in the bottom center part of the setup is used to connect the 20 V operating voltage and GND cables. 'Can on/off' switch connects the operating voltage to the CAN-bus. Shutting the bus down before stopping the control software prevents the can from getting in error mode. All cables leave the board through strain reliefs to prevent the accidental disconnections.

APPENDIX B: THE MEASUREMENT-BASED DIMENSIONS AND WEIGHTS OF THE EXCAVATOR PARTS

The 3D-model of the excavator is built on PTC Creo modeling software. The dimensions of the model are based on physical measurements. This appendix includes the joint locations and weights of all solid parts of the front hoe, and the cylinder dimensions. Locations are presented in relation to the origin, which is the first joint of the part, and these values can easily be used to reproduce the front hoe geometry in SimMechanics.

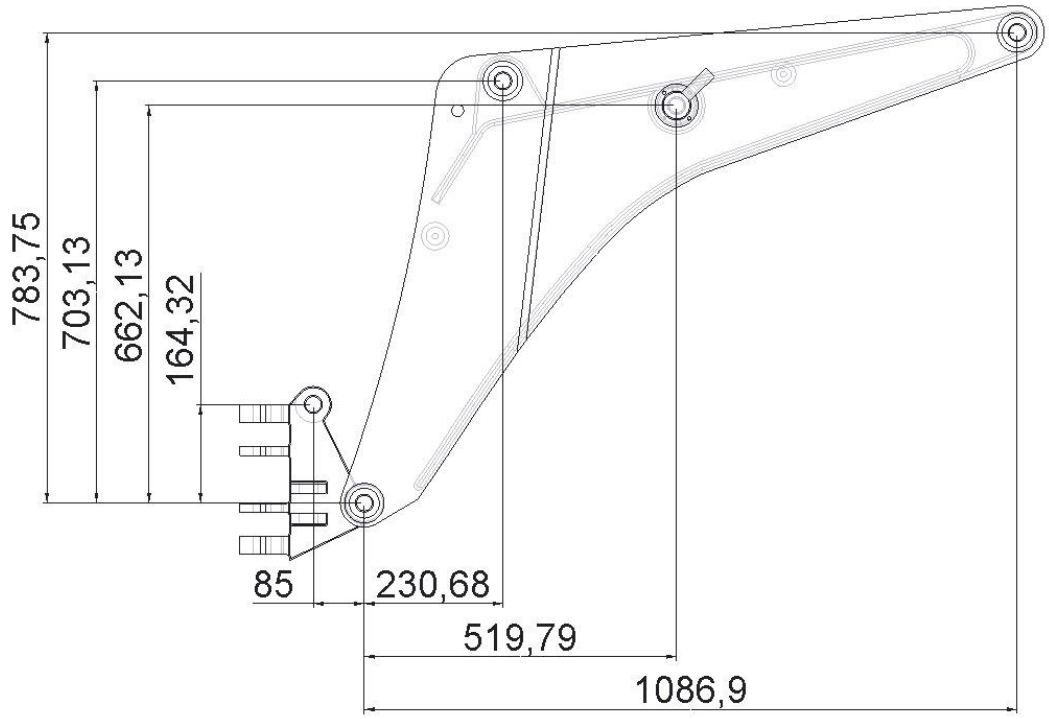

Figure 38: Joint locations of the kingpost and the boom

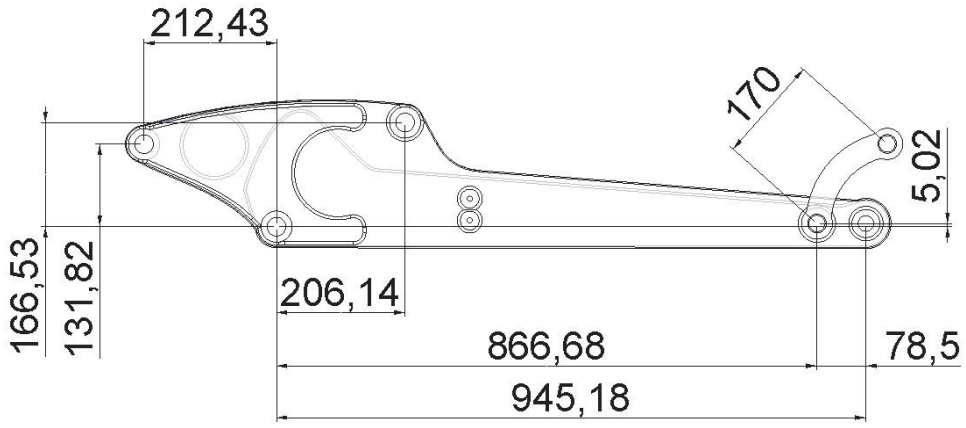

Figure 39: Joint locations of the arm and the first linkage rod

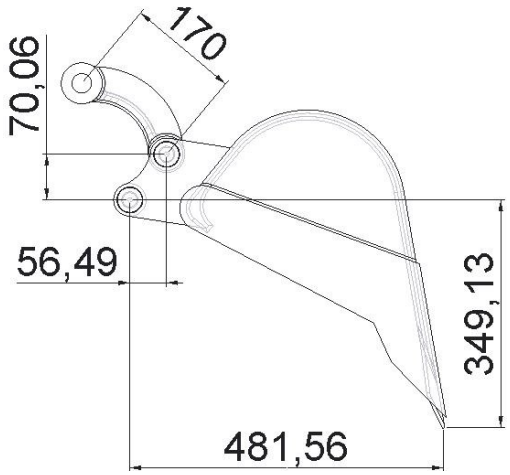

Figure 40: Joint locations of the bucket and the second linkage rod

The dimensions are measured using a caliper for shorter and a measuring tape for longer dimensions, so an error of approximately ± 1 mm is conceivable. The cylinder lengths and dry weights (without oil) are presented in Table 10.

Table 10: Cylinder lengths and weights

Cylinder	Piston diameter [mm]	Rod diameter [mm]	Min length [mm]	Stroke [mm]	Max length [mm]	Dry weight [kg]
Boom	60	30	695.0	324.6	1019.6	16.0
Arm	50	30	667.0	408.0	1075.0	11.0
Bucket	50	30	525.0	288.0	813.0	9.0

The masses of the solid parts are collected in Table 11.

Table 11: Structure masses

Part	Mass [kg]
Boom	59.5
Arm	28.0
Bucket	30.0
Linkages	10.0
Boom accessories	4.5

Boom accessories refer to working light and piping for auxiliary functions (bucket tilt). These are currently disconnected from the excavator.

APPENDIX C: MODEL PARAMETERS

Hydraulic parameters

```
pS = 180e5;                         % Nominal supply pressure [Pa]
pT = 0;                             % Tank pressure [Pa]
Free_air = 0                        % Amount of free air in the system

%% Volume parameters

Volume.rho = 870;                   % Density of the fluid [kg/m^3]
Volume.B = 1500e6;                  % Oil bulk modulus [Pa]

%% Hose parameters

Hose.B_eff = 400e6;                 % Hose bulk modulus [Pa]

Hose.Arm_A.xi = 2.4;                % Hose single friction factor [-]
Hose.Arm_A.l = 3.0;                 % Hose length [m]
Hose.Arm_A.d = 0.006;               % Hose inner diameter [m]
Hose.Arm_B.xi = 2.4;                % Hose single friction factor [-]
Hose.Arm_B.l = 3.0;                 % Hose length [m]
Hose.Arm_B.d = 0.006;               % Hose inner diameter [m]

Hose.Boom_A.xi = 2.4;               % Hose single friction factor [-]
Hose.Boom_A.l = 2.8;                % Hose length [m]
Hose.Boom_A.d = 0.006;              % Hose inner diameter [m]
Hose.Boom_B.xi = 2.4;               % Hose single friction factor [-]
Hose.Boom_B.l = 2.8;                % Hose length [m]
Hose.Boom_B.d = 0.006;              % Hose inner diameter [m]

Hose.Bucket_A.xi = 2.4;             % Hose single friction factor [-]
Hose.Bucket_A.l = 3.8;              % Hose length [m]
Hose.Bucket_A.d = 0.006;            % Hose inner diameter [m]
Hose.Bucket_B.xi = 2.4;             % Hose single friction factor [-]
Hose.Bucket_B.l = 3.8;              % Hose length [m]
Hose.Bucket_B.d = 0.006;            % Hose inner diameter [m]

Hose.Pump.xi = 10;                  % Hose single friction factor [-]
Hose.Pump.l = 2.8;                  % Hose length [m]
Hose.Pump.d = 0.0095;               % Hose inner diameter [m]

%% Valve parameters

Valve.omega_n = 30;                 % Spool natural frequency [rad/s]
Valve.xi = 0.8;                     % Spool damping ratio [-]
Valve.pN = 10e5;                    % Nominal pressure difference [Pa]
Valve.ptr = 1e5;                    % Transition pressure

Valve.pN_PRV = 125e5;               % Nominal pressure difference [Pa]
Valve.QN_PRV = 80/60000;            % Nominal flow [m^3/s]

Valve.pN_PAS = 20e5;                % Nominal pressure difference [Pa]
Valve.QN_PAS = 20/60000;            % Nominal flow [m^3/s]

Valve.QN_bucket = 5.4/60000;        % Nominal flow [m^3/s]
Valve.QN_T_bucket = 6.1/60000;      % Nominal flow to tank [m^3/s]
Valve.QN_arm = 5.3/60000;           % Nominal flow [m^3/s]
```

```
Valve.QN_T_arm = 6.2/60000;         % Nominal flow to tank [m^3/s]
Valve.QN_boom = 5.6/60000;          % Nominal flow [m^3/s]
Valve.QN_T_boom = 6.1/60000;        % Nominal flow to tank [m^3/s]

%% Cylinder parameters

%% Boom cylinder 60/30-300

Boom_cyl.D = 0.060;                 % Cylinder piston diameter [m]
Boom_cyl.d = 0.030;                 % Cylinder rod diameter [m]
Boom_cyl.x_max = 0.3246;            % Cylinder stroke [m]
Boom_cyl.A_A = pi*Boom_cyl.D^2/4;   % Cylinder area (A-side) [m^2]
Boom_cyl.A_B = Boom_cyl.A_A - pi*Boom_cyl.d^2/4;
                                    % Cylinder area (B-side) [m^2]
Boom_cyl.V_0A = 0.1e-3;             % Dead volume (A-side) [m^3]
Boom_cyl.V_0B = 0.1e-3;             % Dead volume (B-side) [m^3]
Boom_cyl.B_eff = 1200e6;            % Cylinder effective bulk modulus [N/m^2]
Boom_cyl.p_init.A = pT;             % Initial pressure in chamber A [Pa];
Boom_cyl.p_init.B = 6.2e6;          % Initial pressure in chamber A [Pa];

Boom_cyl.v_s = 0.001;               % Stribeck velocity [m/s]
Boom_cyl.F_c = 200;                 % Coulomb friction [N]
Boom_cyl.F_s = 800;                 % Static friction [N]
Boom_cyl.sigma_0 = 1.6e6;           % Stiffness of bristles [N/m]
Boom_cyl.sigma_1  = 5e3;            % Damping coefficient [Ns/m]
Boom_cyl.sigma_2  = 5e3;            % Viscous friction coefficient [Ns/m]

Boom_cyl.x_max_collision = 0.001;   % Maximum displacement the plunger is
                                    allowed to go over natural movement [m]
Boom_cyl.m_eff = 100;           % Effective inertial load of the cylinder [kg]
Boom_cyl.K_end = pS*Boom_cyl.A_A/Boom_cyl.x_max_collision;
                                    % Spring constant of a cylinder end [-]
Boom_cyl.b_end = 0.7*(Boom_cyl.K_end*Boom_cyl.m_eff)^(1/2);
                                    % Damping term of a cylinder end [-]

%% Arm cylinder 50/30-430

Arm_cyl.D = 0.050;                  % Cylinder piston diameter [m]
Arm_cyl.d = 0.030;                  % Cylinder rod diameter [m]
Arm_cyl.x_max = 0.408;              % Cylinder stroke [m]
Arm_cyl.A_A = pi*Arm_cyl.D^2/4;     % Cylinder piston area (A-side) [m^2]
Arm_cyl.A_B = Arm_cyl.A_A - pi*Arm_cyl.d^2/4;
                                    % Cylinder piston area (B-side) [m^2]
Arm_cyl.V_0A = 0.1e-3;              % Dead volume (A-side) [m^3]
Arm_cyl.V_0B = 0.1e-3;              % Dead volume (B-side) [m^3]
Arm_cyl.B_eff = 1000e6;             % Cylinder effective bulk modulus [N/m^2]
Arm_cyl.p_init.A = pT;              % Initial pressure in chamber A [Pa];
Arm_cyl.p_init.B = 1.2e6;           % Initial pressure in chamber A [Pa];

Arm_cyl.v_s = 0.001;                % Stribeck velocity [m/s]
Arm_cyl.F_c = 200;                  % Coulomb friction [N]
Arm_cyl.F_s = 400;                  % Static friction [N]
Arm_cyl.sigma_0 = 1.6e6;            % Stiffness of bristles [N/m]
Arm_cyl.sigma_1   = 5e3;            % Damping coefficient [Ns/m]
Arm_cyl.sigma_2   = 5e3;            % Viscous friction coefficient [Ns/m]

Arm_cyl.x_max_collision = 0.002;    % Maximum displacement the plunger is
                                    allowed to go over natural movement [m]
Arm_cyl.m_eff = 100;            % Effective inertial load of the cylinder [kg]
```

```
Arm_cyl.K_end = pS*Arm_cyl.A_A/Arm_cyl.x_max_collision;
                                % Spring constant of a cylinder end [-]
Arm_cyl.b_end = 0.7*(Arm_cyl.K_end*Arm_cyl.m_eff)^(1/2);
                                % Damping term of a cylinder end [-]

%% Bucket cylinder 50/30-300

Bucket_cyl.D = 0.050;           % Cylinder piston diameter [m]
Bucket_cyl.d = 0.030;           % Cylinder rod diameter [m]
Bucket_cyl.x_max = 0.288;       % Cylinder stroke [m]
Bucket_cyl.A_A = pi*Bucket_cyl.D^2/4;
                                % Cylinder piston area (A-side) [m^2]
Bucket_cyl.A_B = Bucket_cyl.A_A - pi*Bucket_cyl.d^2/4;
                                % Cylinder piston area (B-side) [m^2]
Bucket_cyl.V_0A = 0.1e-3;       % Dead volume (A-side) [m^3]
Bucket_cyl.V_0B = 0.1e-3;       % Dead volume (B-side) [m^3]
Bucket_cyl.B_eff = 1000e6;      % Cylinder effective bulk modulus [N/m^2]
Bucket_cyl.p_init.A = 3.5e5;    % Initial pressure in chamber A [Pa];
Bucket_cyl.p_init.B = pT;       % Initial pressure in chamber A [Pa];

Bucket_cyl.v_s = 0.001;         % Stribeck velocity [m/s]
Bucket_cyl.F_c = 200;           % Coulomb friction [N]
Bucket_cyl.F_s = 400;           % Static friction [N]
Bucket_cyl.sigma_0 = 1.6e6;     % Stiffness of bristles [N/m]
Bucket_cyl.sigma_1 = 5e3;       % Damping coefficient [Ns/m]
Bucket_cyl.sigma_2 = 2e3;       % Viscous friction coefficient [Ns/m]

Bucket_cyl.x_max_collision = 0.002;
                                % Maximum displacement the plunger is
                                allowed to go over natural movement [m]
Bucket_cyl.m_eff = 100;      % Effective inertial load of the cylinder [kg]
Bucket_cyl.K_end = pS*Bucket_cyl.A_A/Bucket_cyl.x_max_collision;
                                % Spring constant of a cylinder end [-]
Bucket_cyl.b_end = 0.7*(Bucket_cyl.K_end*Bucket_cyl.m_eff)^(1/2);
                                % Damping term of a cylinder end [-]

%% Pump parameters

Pump.V = 6e-6;                  % Pump volume [m^3]
Pump.B_eff = 500e6;             % Pump effective bulk modulus [N/m^2]

%% Controller

Controller.K_p_boom = 100;      % Controller gain
Controller.K_p_arm = 100;       % Controller gain
Controller.K_p_bucket = 100;    % Controller gain
```

Multibody model parameters

```
%% Initial positions

Cyl1.x_init = 0.155;            % Boom initial position [0..324.6]
Cyl2.x_init = 0.001;            % Arm initial position [0..408]
Cyl3.x_init = 0.07;             % Bucket initial position [0..288]

%% Kingpost solid

Kingpost.step = 'kingpost.stp';     % Name of STEP-file
Kingpost.m = 15;                    % Mass [kg]
```

```
%% Rigid transform from kingpost solid to Boom solid

Boom.j = [0.085 0 0];

%% Rigid transform from kingpost to Boom cylinder

Boom_rod.j = [0 0.165 0];

%% Boom solid

Boom.step = 'boom.stp';            % Name of STEP-file
Boom.m = 59.5 + 1.7;               % Measured mass + weight of hoses [kg]

%% Rigid transform from Boom solid to Boom cylinder

Boom_cyl.j = [0.79857 0.26625 0];

%% Boom cylinder

Cyl1.l = 0.5098;                   % Cylinder length [m]
Cyl1.r = 0.030;                    % Piston radius [m]
Cyl1.m = 16.0/2 + 0.665;           % Measured mass + weight of oil [kg]
Pist1.r = 0.015; % Rod radius [m]
Pist1.l = 0.5098;   % Rod length [m]
Pist1.m = 16.0/2;   % Measured mass [kg]

%% Rigid transform from Boom solid to Arm solid

Arm.j = [1.33886 0.05534 0];

%% Arm solid

Arm.step = 'arm.stp';              % Name of STEP-file
Arm.m = 28;                        % Measured value [kg]

%% Rigid transform from Boom solid to Arm cylinder

Arm_cyl.j = [0.57987 0.45973 0];

%% Arm cylinder

Cyl2.l = 0.5375;                   % Cylinder length [m]
Cyl2.r = 0.025;                    % Piston radius [m]
Cyl2.m = 11.0/2 + 0.572;           % Measured mass + weight of oil [kg]

Pist2.r = 0.015;                   % Rod radius [m]
Pist2.l = Cyl2.l;                  % Rod length [m]
Pist2.m = 11.0/2;                  % Measured mass [kg]

%% Rigid transform from Arm solid to Arm cylinder

Arm_rod.j = [-0.21260 0.13153 0];

%% Rigid transform from Arm solid to Bucket cylinder

Bucket_cyl.j = [0.20591 0.16681 0];

%% Bucket cylinder
```

```
Cyl3.l = 0.4065;                    % Cylinder length [m]
Cyl3.r = 0.025;                     % Piston radius [m]
Cyl3.m = 9.0/2 + 0.406;             % Measured mass + weight of oil [kg]

Pist3.r = 0.015;                    % Rod radius [m]
Pist3.l = 0.4065;                   % Rod length [m]
Pist3.m = 9.0/2;                    % Measured mass [kg]

%% Link 1 solid
Link1.step = 'link1.stp';           % Name of STEP-file
Link1.m = 5;                        % Measured value [kg]

%% Rigid transform from Arm solid to Link1

Link1.j = [0.86666 0.00617 0];

%% Bucket solid

Bucket.step = 'bucket.stp';         % Name of STEP-file
Bucket.m = 30;                      % Measured value [kg]

%% Rigid transform from Arm solid to Bucket

Bucket.j = [0.94516 0.00617 0];

%% Link 2 solid

Link2.step = 'link2.stp';           % Name of STEP-file
Link2.m = 5;                        % Measured value [kg]

%% Rigid transform from Bucket solid to Link2 joint

Link2.j = [0.090 0 0];

%% Pin 1

Pin_1.l = 0.200;                    % Pin length [m]
Pin_1.r = 0.015;                    % Pin radius [m]
Pin_1.m = 1.076;                    % Pin mass [kg]

%% Pin 2

Pin_2.l = 0.120;                    % Pin length [m]
Pin_2.r = 0.015;                    % Pin radius [m]
Pin_2.m = 0.628;                    % Pin mass [kg]

%% Pin 3

Pin_3.l = 0.200;                    % Pin length [m]
Pin_3.r = 0.015;                    % Pin radius [m]
Pin_3.m = 1.076;                    % Pin mass [kg]

%% Pin 4

Pin_4.l = 0.200;                    % Pin length [m]
Pin_4.r = 0.015;                    % Pin radius [m]
Pin_4.m = 1.076;                    % Pin mass [kg]
```

```
%% Pin 5

Pin_5.l = 0.120;                    % Pin length [m]
Pin_5.r = 0.015;                    % Pin radius [m]
Pin_5.m = 0.657;                    % Pin mass [kg]

%% Pin 6

Pin_6.l = 0.200;                    % Pin length [m]
Pin_6.r = 0.015;                    % Pin radius [m]
Pin_6.m = 1.076;                    % Pin mass [kg]

%% Pin 7

Pin_7.l = 0.120;                    % Pin length [m]
Pin_7.r = 0.015;                    % Pin radius [m]
Pin_7.m = 0.657;                    % Pin mass [kg]

%% Pin 8

Pin_8.l = 0.150;                    % Pin length [m]
Pin_8.r = 0.015;                    % Pin radius [m]
Pin_8.m = 0.827;                    % Pin mass [kg]

%% Pin 9

Pin_9.l = 0.180;                    % Pin length [m]
Pin_9.r = 0.015;                    % Pin radius [m]
Pin_9.m = 0.741;                    % Pin mass [kg]

%% Pin 10

Pin_10.l = 0.150;                   % Pin length [m]
Pin_10.r = 0.015;                   % Pin radius [m]
Pin_10.m = 0.827;                   % Pin mass [kg]

%% Pin 11

Pin_11.l = 0.180;                   % Pin length [m]
Pin_11.r = 0.015;                   % Pin radius [m]
Pin_11.m = 0.741;                   % Pin mass [kg]

%% Colours

Color.JCB = [1.0 0.8 0.0];          % JCB Yellow
Color.steel = [0.7 0.7 0.7];
Color.black = [0.2 0.2 0.2];
```

DDH model parameters

```
DDH parameters by Järf, 2009.

gain = 1;
mass = 0;                           % Modified by VS 6.7.2107

%% General parameters
m_chain = 2.88;                     % Mass of chain [kg]
m_holder = 5.44;                    % Mass of holder [kg]
m = mass+m_chain+m_holder;          % Mass of plates + weight of holder
```

```
g = 9.81;                           % Gravitational acceleration [m/s]
B_eff = 0.09e9;                     % Effective bulk modulus [n/m^2 ~ Pa) -
                                    Only used in constant bulk modulus model
temperature = 273.15+20.5;          % Ambient temperature in Kelvin

%% Fluid parameters
rho = 860;                          % Density of fluid [kg/m^3]

% Bulk modulus model

n = 1.4;                            % Polytropic constant
p_0 = 1e5;                          % Inital pressure (athmoshperic pressure)
X_0 = 4.5/100;                      % Gas content of oil (free air)
B_liq = 1.4e9;                      % Bulk modulus of liquid [litterature]
B_min = 0.1*1.4e7;                  % Fix the bulk modulus to minimum value
B_0 = B_liq;                        % Used only in extended Wylie-Yu
                                    [Litterature]
B_1 = 11.4;                         % Used only in extended Wylie-Yu
                                    [Litterature]

%% Pump parameters

% A-side pump

D_pA = 22.8*1e-6;                   % Displacement of A-side pump [m^3/rev]
K_lamA = -2.65548e-013;             % Laminar leak parameter
                                    [m^3/s*bar][measured]
K_turbA = 4.43707e-009;             %Turbulent leak parameter
                                    [m^3/s*sqrt(bar)][measured]
K_tempA =  6.30177e-005;            % Temperature leak parameter [measured]
alpha_A = -0.000361545;             % Intecept from regression
eta_hmA =  0.85;                    % Hydro-mechanical efficiency
                                    [%][estimated from datasheet]
eta_vA = 1;                         % Volumetric efficiency (leave as 1 is the
                                    leak model is used)

% B-side pump

D_pB = 14.4*1e-6;                   % Displacement of B-side pump [m^3/rev]
K_lamB =  6.09061e-013;             % Laminar leak parameter
                                    [m^3/s*bar][measured]
K_turbB =  1.95831e-009;            % Turbulent leak parameter
                                    [m^3/s*sqrt(bar)][measured]
K_tempB =  4.11706e-005;            % Temperature leak parameter [measured]
alpha_B =   -0.000235770;           % Intecept from regression
eta_hmB = 0.85;                     % Hydro-mechanical efficiency
                                    [%][estimated]
eta_vB = 1;                         % Volumetric efficiency (leave as 1 is the
                                    leak model is used)

%% Hose parameters

% Hose between A-pump and A-chamber

d_hoseA = 10/1000;                  % Diameter of hose [measured]
l_hoseA = 2;                        % Length of hose [measured]
V_hoseA = (pi/4)*d_hoseA^2*l_hoseA; %Volume of hose

% Hose between B-pump and B-chamber
```

```
d_hoseB = 10/1000;                  % Diameter of hose [measured]
l_hoseB = 2;                        % Length of hose [measured]
V_hoseB = (pi/4)*d_hoseB^2*l_hoseB; %Volume of hose

%% Accumulator parameters

p_pre = 10e5;                       % Precharge pressure [bar -> Pa]
V_Acc = 0.7/1000;                   % Total accumulator volume [l -> m^3]
V_fluid0 = 0;                       % Initial accumulator volume
K_s = 5e10 ;                        % Hard-stop stiffness coeff.
                                    [Pa/m^3](litterature)
K_d = 0e9;                          % Hard-stop damping coeff. [Pa*s/m^6]
                                    (litterature)
V_dead_Acc = 0.1*V_Acc;             % Accumulator dead volume (estimated)
p_atm = 1e5;                        % Atmospheric pressure [bar]

d_oAcc = 3/1000;                    % Accumulator inlet diameter [measured]
A_oAcc = (pi/4)*d_oAcc^2;           % Accumulator inlet area [calculated]

%% Controller                       % Added by VS 6.7.2107

Controller.K_p_DDH_Bucket = 5e4;
Controller.K_p_DDH_Arm = 5e4;
Controller.K_p_DDH_Boom = 5e4;

Controller.max_speed = 1500;
Controller.min_speed = -1500;
```